

THERMODYNAMICS AND KINETICS OF
DNA ORIGAMI CROSS-TILE ARRAY FORMATION

by

Brett Michael Ward

A thesis

submitted in partial fulfillment

of the requirements for the degree of

Master of Science in Materials Science and Engineering

Boise State University

December 2017

© 2017

Brett Michael Ward

ALL RIGHTS RESERVED

BOISE STATE UNIVERSITY GRADUATE COLLEGE

DEFENSE COMMITTEE AND FINAL READING APPROVALS

of the thesis submitted by

Brett Michael Ward

Thesis Title: Thermodynamics and Kinetics of DNA Origami Cross-Tile Array
Formation

Date of Final Oral Examination: 28 February 2017

The following individuals read and discussed the thesis submitted by student Brett Michael Ward, and they evaluated his presentation and response to questions during the final oral examination. They found that the student passed the final oral examination.

Elton Graugnard, Ph.D.	Chair, Supervisory Committee
William L. Hughes, Ph.D.	Member, Supervisory Committee
Wan Kuang, Ph.D.	Member, Supervisory Committee
Bernard Yurke, Ph.D.	Member, Supervisory Committee

The final reading approval of the thesis was granted by Elton Graugnard, Ph.D., Chair of the Supervisory Committee. The thesis was approved by the Graduate College.

DEDICATION

To Hayley. Thank you for always reminding me to smile.

ACKNOWLEDGMENTS

The work described within this text is the culmination of the many efforts put forth by my mentors, predecessors, peers, family, and friends. It was through their support, insight, and encouragement that this endeavor was made possible. I would like to acknowledge and sincerely thank the individuals whose contributions have been invaluable to my progress thus far and whose influence will remain with me for life.

My committee members, Dr. Will Hughes, Dr. Wan Kuang, and especially Dr. Bernie Yurke for their insight, direction, critiques, and considerable investment of time in guiding this project along. Dr. Elton Graugnard for his tutelage, patience, guidance and the occasional gentle nudge to help me reach my goals.

The Micron School of Materials Science and Engineering for providing the opportunity to pursue a graduate level education. Stephanie Moran and Chad Watson for all their help with administrative tasks throughout the project. A large portion of the research for this thesis was made possible by NASA ISGC Grant NNX15A104H.

The Surface Science Laboratory staff, Kari Livingston, Jesse Schimpf, Corey Efaw, and Dr. Paul Davis for their time spent characterizing my samples and with training. Dr. Natalya Hallstrom of the W. M. Keck Laboratory and my fellow students, Blake Rapp, Sadao Takabayashi, Will Klein, Chris Green, and Donald Kellis for their training, insights, and ideas inside and out of the lab.

A special thanks to Brittany Kohoutek and Michael Tobiason for keeping me motivated throughout this entire experience. Jeff Ward and Fred Burton for being the

ones to inspire me to pursue math and science and Mom and Dad for encouraging me in everything I do.

ABSTRACT

As the cost to continue scaling photolithography to pattern smaller semiconducting devices increases exponentially, new materials and fabrication approaches are being sought to extend and enhance current capabilities. DNA nanostructures have been identified as a promising material for patterning nanoscale devices, and several studies have demonstrated the ability to program DNA nanostructures to self-assemble into large scale arrays. These DNA arrays can be designed to create the patterns necessary for fabricating semiconductor device features. However, these structures are far from ideal and contain a number of defects that limit the adoption of this approach for manufacturing. In order to create large defect-free DNA arrays, further study is needed into the fundamental mechanisms governing array formation. Toward this goal, the thermodynamics and kinetics of DNA array formation were investigated using a DNA origami cross-tile that assembles into arrays through DNA hybridization. The assembly of dimers, quadramers, and unbound arrays in solution from monomers with complementary dye and quencher labeled hybridization interfaces was monitored by observing the change in fluorescence of the solution as a function of temperature and over time under varying buffer conditions and temperatures. The melting temperature of each structure was measured and generally increased with an increasing number of active sticky-ends per monomer. Values for standard thermodynamic parameters were determined for each array design. The reaction kinetics data were fit with a second order reaction model, and the effective reaction rate increased with

increasing buffer magnesium concentrations and increasing temperatures. Finally, it was determined that large, unbounded 2D DNA origami cross-tile arrays sediment out of solution in only a few hours. The findings of this study provide insight into the mechanisms of DNA array formation and establish practical ranges for key processing parameters.

TABLE OF CONTENTS

DEDICATION	iv
ACKNOWLEDGMENTS	v
ABSTRACT.....	vii
LIST OF FIGURES	xii
LIST OF TABLES	xvi
LIST OF ABBREVIATIONS.....	xvii
CHAPTER ONE: INTRODUCTION.....	1
CHAPTER TWO: BACKGROUND	4
2.1 Scaling DNA Self-Assembly	4
2.2 DNA Origami Tiling.....	5
2.2.1 Surface-Assisted DNA Origami Tiling.....	5
2.2.2 Solution Based DNA Origami Tiling	6
2.2.3 Previous Studies of DNA Thermodynamics and Kinetics.....	6
CHAPTER THREE: EXPERIMENTAL METHODS	11
3.1 DNA Origami and Duplex	11
3.1.1 DNA Cross-Tile Design.....	11
3.1.2 DNA Cross-Tile Design Modification for Array Formation	12
3.1.3 Edge Staple Modifications for Dynamic Fluorescence Monitoring .	12
3.1.4 DNA Cross-Tile Synthesis.....	13

3.1.5 DNA Cross-Tile Concentration Measurement.....	14
3.2 DNA Melting	14
3.2.1 DNA Cross-Tile Melting	15
3.2.2 Array Structure Melting.....	15
3.3 Kinetics Measurements.....	16
3.3.1 Temperature Dependent Kinetics Measurements	16
3.3.2 Magnesium Concentration Dependent Kinetics Measurements	16
3.4 Atomic Force Microscopy	17
CHAPTER FOUR: RESULTS AND DISCUSSION.....	20
4.1 Validation of Design and Methods	20
4.1.1 Fluorescence Quenching of the Simple Duplex Hybridization	20
4.1.2 Fluorescent Signal Quenching as a Result of Dimer Formation.....	21
4.2 Thermodynamic Parameters of Array Structures and Monomers	23
4.2.1 Determining Melting Temperature of DNA Origami Cross-Tile	23
4.2.2 Melting Temperature of DNA Origami Array Structures.....	24
4.2.3 Enthalpy, Entropy, and Gibb's Free Energy of Arrays.....	25
4.3 Effects of Buffer Solution Conditions on Dimer Formation Rates.....	26
4.3.1 Temperature Dependence of Array Formation	26
4.3.2 Effect of Magnesium Concentration on Dimer Formation	27
4.4 Sedimentation of Unbound Arrays	27
CHAPTER FIVE: CONCLUSIONS	40
REFERENCES	42
APPENDIX A.....	45

DNA Origami Cross-Tile and DNA Duplex Designs.....	46
APPENDIX B	48
Kinetics Reaction Curves and 2 nd Order Rate Fits.....	49
APPENDIX C	50
DNA Origami Cross-Tile Staple Lists	51
APPENDIX D.....	64
DNA Origami Annealing Protocol	65

LIST OF FIGURES

Figure 2.1.	<p>Example of the self-assembly of complex 3D structures from unique oligos. A) A single ssDNA “brick”. B) Schematic of the hybridization between two complimentary bricks. C) A model of the helical structure within a 3D brick structure. Individual unique strands are represented by different colors. D) A Lego-like model of 3D brick assembly. E,F) Mixing and/or omitting individual components of a 3D canvas during assembly result in specific complex structures. Figure borrowed from reference 37. 8</p>
Figure 2.2.	<p>Schematics and AFM images of small dsDNA tiles and the 2D arrays formed by their self-assembly. (a) A two tile system forming an unrestricted 2D array. (b) Two systems of unique tiles designed with specific binding regions to form the two different structures shown in the AFM image. (c) A large, complex 2D binary counter ribbon self-assembled from a system of dsDNA tiles. Figure borrowed from reference 30..... 9</p>
Figure 2.3.	<p>Schematic of a multi-scaffold “origami of origami”. Individual DNA origami tiles (top left) and scaffold frameworks (top right) are folded independently using different scaffold and staple strands. When the tiles and frameworks are combined in solution they form a pre-determined superstructure. Figure borrowed from reference 40. 10</p>
Figure 3.1.	<p>Diagram of A-Tile and B-Tile after folding. The B-Tile is oriented 90° clockwise relative to the A-Tile as defined by the hybridization interfaces 1, 2, 1', and 2'. The sticky-end sequences are designed so that 1 and 2 are complementary only to 1' and 2' respectively. This creates two-fold symmetry in the cross-tiles when all four tile arms are active..... 17</p>
Figure 3.2.	<p>Schematics of the four array structures studied. (a, b) Activating one tile arm of either the 1-1' or 2-2' hybridization interfaces on each tile creates two unique dimer structures. (c) Activating one set of the 1-1' and 2-2' interfaces creates a 2x2 array. (d) Activating all four interfaces of each tile results in an unbounded array. 18</p>
Figure 3.3.	<p>Schematic of a hybridization interface a) before and b) after hybridization. Two sticky-ends (red) on each tile arm are modified with either a</p>

fluorophore (gold star) or quencher (black circle). After hybridization, fluorescence from the tile arm is largely quenched which enables monitoring of array formation by fluorescence. 19

Figure 4.1. Fluorescence Intensity vs Time of a solution of CO-B-L1-Cy5-Ext dye strand and CO-B-L1-comp before and after the injection of the CO-A-R1-RQ strand. The initial fluorescence of the dye/complementary strand solution at [DNA] = 5 nM was measured for 300 seconds to establish a pre-injection fluorescence value. At t = 300 s, the quencher strand was added to the solution, bringing the [DNA] to 4.75 nM. Applying this dilution factor to the pre-injection fluorescence measurement provided an initial fluorescence parameter for our second order reaction fit. The calculated association rate for this simple duplex reaction is $k_{on} = 1.43 \times 10^6 \text{ M}^{-1}\text{s}^{-1}$ 29

Figure 4.2. AFM images, the corresponding fluorescence value of the solution, and the count of cross-tiles as monomers and dimers of samples prepared at sequential time intervals (red arrows) from a 2-2' dimer formation reaction. a) Before injection only one tile species is present in solution. A pre-injection fluorescence value is measured at [DNA] = 1 nM and all the cross-tiles present in AFM exist as monomers. b) At injection (t = 0), the fluorescence of the solution with [DNA] = 2 nM has jumped due to the increase in the number of cross-tile monomers present. This fluorescence value is taken as the initial fluorescent parameter for the second order reaction fit. AFM shows that over 99% of the cross-tiles present exist in monomer form as there has been insufficient time for dimer formation to occur. c) At t = 25 minutes the total fluorescence of the solution has decreased to 70% of its initial value. Concurrently, AFM images show that ~30% of the cross-tiles have dimerized. d) At t = 240 minutes the total fluorescence has decreased to 30% of the initial value and 70% of the cross-tiles in AFM have dimerized. 30

Figure 4.3. Cross-Tile Melting Curve. The absorbance of 260 nm light vs temperature of a 5 nM sample of A-Tile monomers. Upper and lower baseline equations are established from the linear regions of the curve at either temperature extremes. From the two baselines, a median line can be defined and T_m is defined as the temperature at which the median line crosses the measured data⁴⁸. The melting temperature of the A-Tile is measured at 52.5 °C. Since the B-Tile differs from the A-Tile by only 24 unique edge strands, this is taken to be the melting temperature of both monomers..... 31

Figure 4.4. The effect of temperature on fluorescence of the dye strand on the cross-tile monomers. a) The raw melting curve data of an A-Tile monomer solution. The shape of the monomer solution curve indicates that as temperature increases, the base fluorescence signal of the dye labelled

cross-tiles decreases. To correct for this effect, the linear fit line of the monomer curve was from the monomer. b) The resulting corrected melting curve accounting for the temperature dependence of the fluorescence signal. The monomer solution fluorescence is consistent over the entire temperature range. All array melting curves were normalized using this method with the linear fit lines coming from their own component single tiles..... 32

Figure 4.5. The schematics, melting temperatures, and analyzed temperature dependent fluorescence corrected melting curves for all a) the 1-1' dimer, b) the 2-2' dimer, c) 2x2 array, and d) the unbounded array structures. As the number of active tile arms per monomer increases, the melting temperature of the resultant array structures increases. Empirically, the increase in melting temperature is 0.56 °C per sticky-end (8 sticky-ends per active tile arm). 33

Figure 4.6. The measured association rates of the four structures as a function of temperature. In general, all the structures see an increase in association rate with increasing temperature. In addition, the association rate increases with an increase in active tile arms per monomer with the unbounded array showing a significant increase in association rate over the three restricted array size designs. 34

Figure 4.7. The buffer magnesium concentration dependence of the 2-2' dimer association rate. As the $[Mg^{++}]$ increases, the association rate increases as well. The association rate can be increased by nearly an order of magnitude with just over a six-fold increase in $[Mg^{++}]$. While the association rate can be significantly increased, it appears to saturate at $5 \times 10^6 M^{-1} s^{-1}$ which is still two orders of magnitude below the calculated diffusion limited association rate for these structures (dotted line). 35

Figure 4.8. Time Lapse of the fluorescence of solutions containing (a) monomer cross-tiles, (b) 2-2' Dimers, and (c) unbound arrays. The monomers and smaller array structures remain suspended in solution for extended time periods but in the case of the unbounded arrays, sedimentation of structures is observed in as little as six hours. At 12 hours, the top of the buffer solution is significantly depleted of structures and a second sedimentation ring has begun to form below the first. After 18 hours the upper portion of the solution contains almost no fluorescent origami structures as both sedimentation rings continue to grow. 36

Figure 4.9. AFM image of structures in a sedimentation ring of an unbound array sample. The small domains of single-crystal origami cross-tile arrays in the polycrystalline aggregate suggest that the arrays reach some critical size before precipitating out of solution and creating areas of high local

origami concentration. Arrays in these areas encounter each other at non-ideal angles and do not have enough mobility to undergo reorientation. . 37

- Figure A.1. Design schematic of DNA cross-tiles (A, B) from caDNAno. The two helical portion (Upper, Lower) of each cross-tile are achieved by rastering the single stranded m13mp18 scaffold strand (blue) parallel to the long axis of each domain. Short staple body stands (green) bind to specific sections of the scaffold strand to fold the scaffold and pin it in place. Staple strands in the middle of the cross-tile (denoted by red 'xx') bind to both helical domains in such a way that the two domains are held perpendicular to each other. Edge staple strands (red) have eight five base-pair single strands, sticky-ends, extending from the cross-tile arms. 46
- Figure A.2. Schematic and sequence design of a) the hybridization of one set of complementary sticky-ends on the 2-2' hybridization interface and b) the simple duplex structure used to verify the fluorescence quenching assay technique. For stability in the duplex structure, the CO-B-L1-Cy5 strand is extended (CO-B-L1-Cy5-Ext) on the 5' end and the CO-B-L1_comp strand is added as a proxy for the portion of the scaffold strand (blue) complementary to the CO-A-R1-RQ and CO-B-L1-Cy5 staples respectively. The result after mixing the three strands is a fluorescence quenched double helix that is 69 base-pairs long. 47
- Figure A.3. Kinetic measurements (black line) and the 2nd order kinetic rate fit (red line) for each of the four array structures at 10 °C, 15 °C, 20 °C, 25 °C, and 30 °C. The R² values for all fits are > 0.98. 49

LIST OF TABLES

Table 4.1.	Calculated Thermodynamic Parameters of Array Formation	38
Table 4.2.	Measured and Calculated Kinetic Parameters of Array Formation	39
Table A.1.	Cross Tile Body Staple Sequences	51
Table A.2.	1-1 Dimer A-Tile Edge Staple Sequences	56
Table A.3.	1-1 Dimer B-Tile Edge Staple Sequences	57
Table A.4.	2-2 Dimer A-Tile Edge Staple Sequences	58
Table A.5.	2-2 Dimer B-Tile Edge Staple Sequences	59
Table A.6.	2x2 Array A-Tile Edge Staple Sequences	60
Table A.7.	2x2 Array B-Tile Edge Staple Sequences.....	61
Table A.8.	UB Array A-Tile Edge Staple Sequences.....	62
Table A.9.	UB Array B-Tile Edge Staple Sequences	63
Table A.10.	Origami Cross Tile Annealing Protocol	65

LIST OF ABBREVIATIONS

nm	Nanometer
EUV	Extreme Ultra-Violet
BCP	Block Copolymer
DNA	Deoxyribonucleic Acid
2D	Two-Dimensional
SEs	Sticky-Ends
bp	Base Pairs
nt	Nucleotide
Mg	Magnesium
Na	Sodium
UB	Unbounded
MgCl ₂	Magnesium Dichloride
TBE	Tris/Borate/EDTA
mM	Millimolar
V	Volt
dsDNA	Double Stranded DNA
°C	Degrees Celsius
cm	Centimeter
T	Temperature
UV-Vis-IR	Ultraviolet-Visible-Infrared

nM	Nanomolar
μL	Microliter
t	Time
NPH ₂ O	Nanopure Water
N ₂	Nitrogen Gas
ssDNA	Single Stranded DNA
T _m	Melting Temperature
ΔH°_{VH}	Van't Hoff Enthalpy of Formation
ΔS°_T	Entropy of Formation at Temperature
ΔG°_T	Gibb's Free Energy of Formation at Temperature
M	Molar
s	Second
m	Meter

CHAPTER ONE: INTRODUCTION

The semiconductor manufacturing industry has nearly reached the lower limits of scalability for photolithography with a 193 nm light source, with production feature sizes on the order of 20 nm¹. Several methods are being pursued to continue scaling nanomanufacturing, such as extreme ultraviolet (EUV) lithography and combining current 193 nm techniques with directed self-assembly of block copolymers (BCPs)^{2,3}. While industry adoption of EUV is inevitable, the cost penalty remains high and the direct advantages are limited¹. Masks made from self-assembled block copolymers (BCPs) have been demonstrated to extend and enhance the limit of current lithographic technology, but defects and limits to design control remain major issues⁴.

As an alternative to BCPs, self-directed DNA assembly is an attractive method for continuing current photolithographic techniques due to its nanoscale feature sizes, diverse programmability, and high addressability⁵. Self-assembled DNA structures can act as a substrate for a variety of nanomaterials and have the potential to achieve spatial resolutions superior to current top-down lithographic methods.⁶⁻¹⁶ To extend the scale of bottom-up DNA origami self-assembly, individual structures are designed such that they will crystallize and form large arrays. This technique, called tiling, is one method to extend the highly addressable nature of individual DNA origami structures from the domain of a hundred nanometers on edge to the tens of microns on edge. DNA nanostructure arrays formed through tiling have been demonstrated in solution and mediated through surface interactions¹⁷⁻²³.

For growth of large-scale 2D origami crystals on a surface, the surface interaction increases as the array grows until the array is immobilized on the surface. This mobility issue is not present in solution based origami tiling, but long-range order within arrays becomes limited by stress-induced curvature within the DNA origami monomers and the greater degrees of freedom for tiling in three dimensions²⁴. In both cases, the thermodynamics and kinetics of DNA origami tiling are not well understood.

Tiling of DNA nanostructures has been achieved using sticky-end hybridization, blunt-end stacking, and combinations of these approaches^{17, 21, 25, 26}. Blunt-end stacking has been employed to provide relatively weak interactions between DNA origami tiles for surface-assisted array formation^{22, 27}. In the first demonstration of a two-dimensional crystal of DNA origami, tiling in solution was achieved by sticky-end hybridization¹⁷, as illustrated in Figure 1, which can yield stronger interactions than blunt-end stacking. For the sticky-end hybridization approach, a number of single stranded “sticky-ends” (SEs) are added to an initial origami design, these sticky-end sequences are programmed to bind to complementary strands on other origami structures with a controlled orientation. By carefully controlling the temperature, 2D crystal arrays ranging in size from hundreds of nanometers to tens of microns form in solution¹⁷. Strict temperature control is necessary to anneal out grain boundaries between crystallites without damaging the individual origami structures, which melt at higher temperatures. The kinetic rates of origami tile dimerization in solution and the thermodynamic stability of the structures are determined by the architecture of the hybridization interface and are unique to each monomer design²⁸. However, the influence of buffer conditions on solution based tiling has yet to be determined and the critical temperatures for large, defect free 2D array

formation are not fully understood. Toward this goal, the objective of this study is to gain insight into the thermodynamics and kinetics of DNA origami cross-tile array formation and the effect of the solution environment.

CHAPTER TWO: BACKGROUND

2.1 Scaling DNA Self-Assembly

Several methods of scaling DNA self-assembly to industry relevant dimensions are being investigated and include self-assembly of large DNA crystals from entirely unique ssDNA strands²⁹, small dsDNA tile assembly³⁰, DNA origami self-assembly using multiple scaffold strands or scaffold strands larger than the standard m13mp18 ssDNA³¹, and tiling of m13mp18 based DNA origami¹⁷. Each method presents its own advantages and disadvantages.

Assembly of large structures using “n” number of unique ssDNA strands (oligos) can produce complex tile structures as seen in Figure 2.1³²⁻³⁷. However, because the complete formation of oligo-based structures is heavily reliant on every single oligo being present, the probability of forming a complete structure decreases as size increases. This leads to low yields of oligo-based self-assembled structures²⁹. Small dsDNA tile assembly takes advantage of periodic growth of a single or small set of subunits into a large array. These dsDNA tiles are often constructed from only a few oligos and through control of their shape and interaction interfaces, 2D and 3D crystals will self-assemble as shown in Figure 2.2. Assembly of useful structures can be difficult as careful control of design and experimental parameters and an increasing number of unique tiles are necessary to assemble large, error-free, tiles with programmed addressability³⁰.

DNA origami is a technique that uses a long ssDNA as a “scaffold” to which a few hundred shorter “staple” oligonucleotides will hybridize³⁸. A scaffold strand can be thought to collect its complementary staple strands in a proper stoichiometric amount resulting in high yields of well-formed nanostructures³⁹. By using larger or multiple scaffold strands, self-assembled structures of arbitrary shape and size with unique addressability are possible⁴⁰. Figure 2.3 shows how additional scaffold strands can be used to create DNA origami superstructures, although creating such structures remains a challenge⁴¹.

2.2 DNA Origami Tiling

DNA origami using a single, standard m13mp18 scaffold strand is limited to self-assembly of structures of only ~100 nm on edge^{38, 39}. To extend the scale of bottom-up DNA origami self-assembly, individual structures can be designed such that they will crystallize and form larger arrays¹⁷. This technique, called tiling, is one method to extend the highly addressable nature of individual DNA origami structures from the domain of a hundred nanometers on edge to the tens of microns on edge.

2.2.1 Surface-Assisted DNA Origami Tiling

For tiling, solutions of DNA origami structures are prepared with high concentrations of cations, typically divalent magnesium. The Mg^{++} ions act to screen the negatively charged DNA backbone and allow for the formation of complex nanostructures. These cations can also act as a bridge between self-assembled DNA origami and a negatively charged surface, such as mica, to bind the structures to the surface. Monovalent cations like sodium (Na^+) also screen the repulsive forces of the negatively charged DNA and surface but to a lesser degree²⁵. By controlling the cation

types and concentrations, the surface mobility of origami structures can be tuned such that individual tiles form large 2D crystals through blunt-end stacking²¹. The charge screening effects of the cations are not strong enough to allow larger origami crystallites to diffuse across the surface, which results in immobile domains, or grains. There is insufficient energy to anneal out dislocations and so large order polycrystalline array formation results.

2.2.2 Solution Based DNA Origami Tiling

Where immobility of larger crystallites hinders large-scale growth of 2D origami single-crystals on a surface, this mobility issue is not present in solution based origami tiling. A number of single stranded “sticky-ends” are added to the initial origami design, these sticky-end sequences are programmed to bind to complementary strands on other origami structures with a controlled orientation. By carefully controlling the temperature, 2D crystal arrays ranging in size from hundreds of nanometers to tens of microns form in solution¹⁷. Strict temperature control is necessary to anneal out grain boundaries between crystallites without damaging the individual origami structures, which melt at higher temperatures.

2.2.3 Previous Studies of DNA Thermodynamics and Kinetics

The thermodynamic parameters of tiling of small double crossover tile (DX tile) monomers show a linear increase in binding energy (ΔG° becoming more negative) with increasing number of sticky-ends per monomer. The binding energy of tiles through sticky-end hybridization is less than the binding energy of the same sticky-ends without tiles, suggesting an additional energy penalty associated with monomer tiling. Furthermore, the kinetic and thermodynamic behaviors of tiles with one or more incorrect

sticky-ends are comparable to those of tiles with sticky-ends omitted by design. That is, mismatched sticky-ends do not create an additional energy barrier but behave as if they are not present in the monomer during tiling⁴².

Zenk et al. showed that forward and reverse reaction rates of dimerization of rectangular origami tiles and the thermodynamic stability of dimer structures are related to the number and length of sticky-end staple strands available to participate in the reaction²⁸. The origami design chosen for that work tends to form long, ribbon-like structures of only a few tiles wide when allowed to crystallize indefinitely. This tiling behavior is common for systems with origami monomers that have only a single helical direction, which preferentially crystallizes parallel to that direction and is not ideal for 2D array formation.

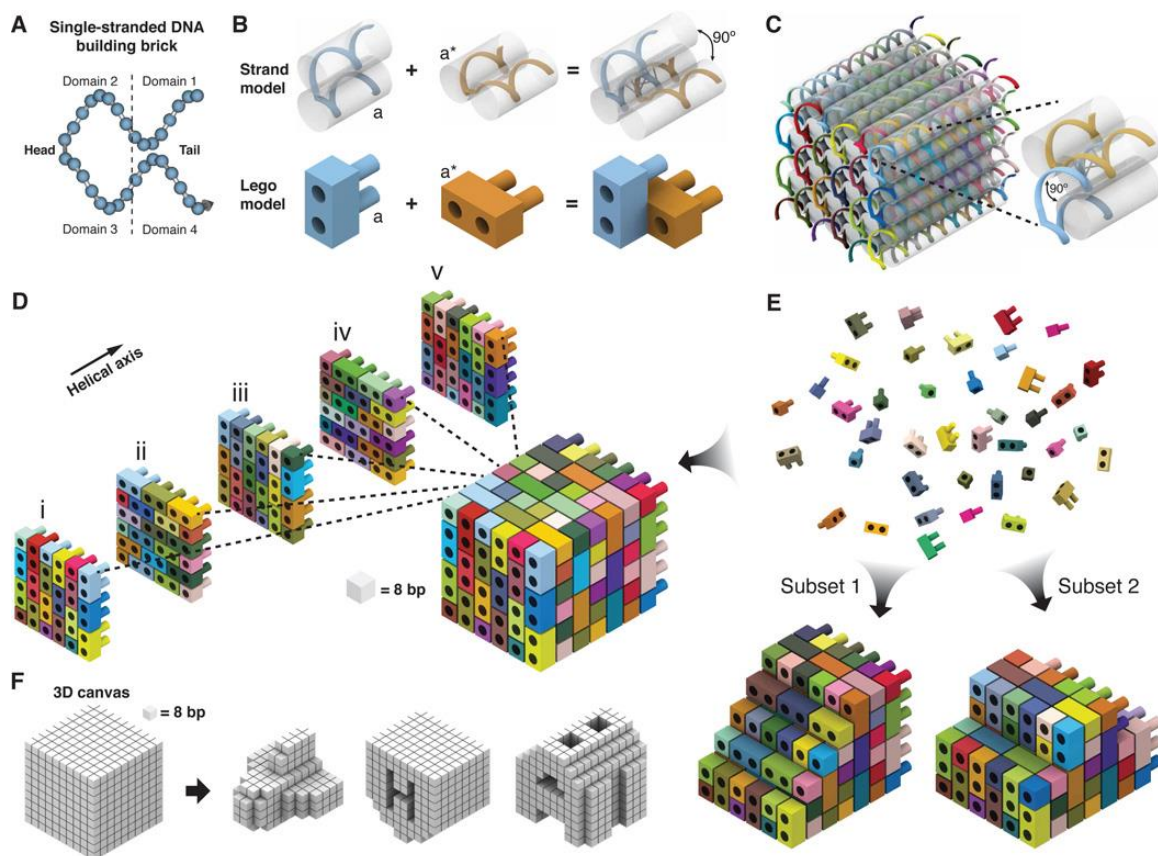


Figure 2.1. Example of the self-assembly of complex 3D structures from unique oligos. **A)** A single ssDNA “brick”. **B)** Schematic of the hybridization between two complimentary bricks. **C)** A model of the helical structure within a 3D brick structure. Individual unique strands are represented by different colors. **D)** A Lego-like model of 3D brick assembly. **E,F)** Mixing and/or omitting individual components of a 3D canvas during assembly result in specific complex structures. Figure borrowed from reference 37.

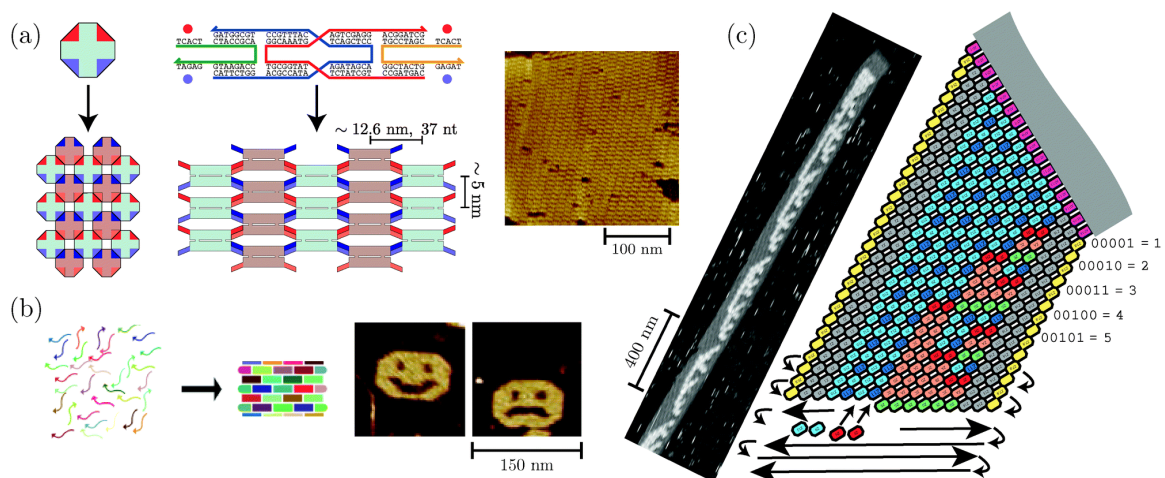


Figure 2.2. Schematics and AFM images of small dsDNA tiles and the 2D arrays formed by their self-assembly. (a) A two tile system forming an unrestricted 2D array. (b) Two systems of unique tiles designed with specific binding regions to form the two different structures shown in the AFM image. (c) A large, complex 2D binary counter ribbon self-assembled from a system of dsDNA tiles. Figured borrowed from reference 30.

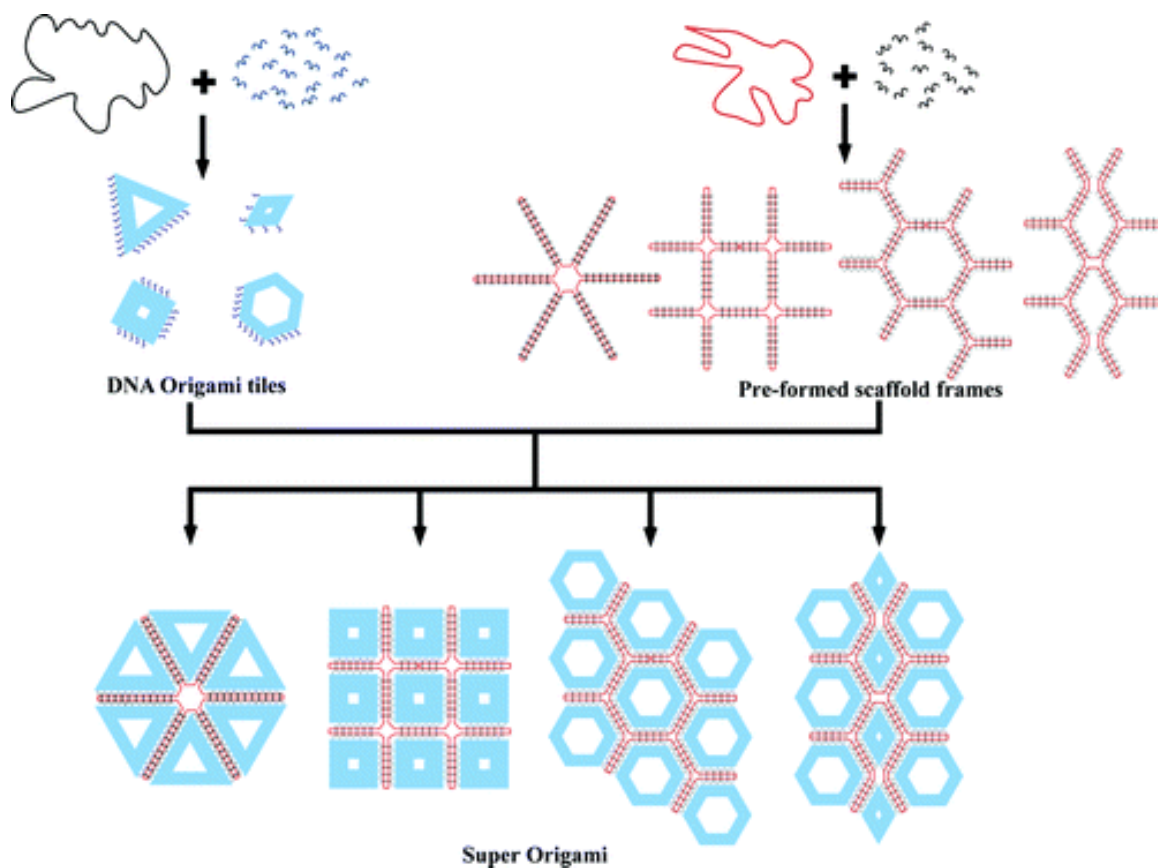


Figure 2.3. Schematic of a multi-scaffold “origami of origami”. Individual DNA origami tiles (top left) and scaffold frameworks (top right) are folded independently using different scaffold and staple strands. When the tiles and frameworks are combined in solution they form a pre-determined superstructure. Figure borrowed from reference 40.

CHAPTER THREE: EXPERIMENTAL METHODS

Described herein are the methods and procedures for the design, assembly, purification, and characterization of the DNA origami tiles used in this study, the kinetic experiments, and the controls used to verify the experimental design.

3.1 DNA Origami and Duplex

The DNA origami design chosen for this study is shown in Figure A.1 and is a cross tile structure with two helical directions oriented 90° relative to each other with the upper portion stacked vertically on the lower portion. These tiles form large 2D crystals in solution as demonstrated by Liu *et al*¹⁷. Modifications were made to Liu's original tile design to account for sequence mismatches, create a dynamic fluorescence monitoring system, and to limit the formation of higher order structures when such structures are not desired. Additionally, a duplex structure was created to validate fluorescent signal quenching with sticky-end hybridization.

3.1.1 DNA Cross-Tile Design

The scaffold consists of a single-stranded m13mp18 genome with 7,249 nt. 177 staple strands define the body of the DNA origami cross tile (Table A.1). To reduce the effect of the inherent curvature of the structure on 2D crystal formation, two independent versions of the cross tile were synthesized and are referred to as A-Tile and B-Tile. Each tile species contains 24 unique edge staples located at the edge of each tile arm. The helical orientation of the top portion of the B-Tile (2') is oriented 90° clockwise to the helical orientation of the top domain of the A-Tile (1) as seen in Figure 3.1.

3.1.2 DNA Cross-Tile Design Modification for Array Formation

When a tile arm is “active” the six edge staple strands are extended to create eight sticky-ends with a length of five bases. The sequences of the sticky-ends are designed to be complementary to the sticky-ends extending from the tile arm on the corresponding tile species. Inactive tile arms have edge staples extended with eight poly-T blocking strands, these blocking strands inhibit blunt-end stacking of tiles to prevent non-specific binding events. Active tile arms create hybridization interfaces that allow the A-Tile and B-Tile to hybridize together to form a higher order structure, the size of which can be controlled by the deactivation of other tile arms on the monomers.

Four different array configurations were designed for this study and schematics of each can be seen in Figure 3.2. The hybridization interfaces of 1-1' and 2-2' were studied separately. By activating only one tile arm of either the 1-1' or 2-2' arms on each monomer and deactivating the other three arms, the result of array formation is a dimer consisting of one A-Tile and one B-Tile. When one arm of each the 1-1' and 2-2' on each cross-tile is active, the final array structures formed are a 2x2. The final structure designed for this study was the case where all four tile arms on each cross-tile are active and unbounded (UB) arrays can form. The sequences of the edge staples are modified based on the desired array architecture. Tables A.2 through A.9 list the edge strands and sequences in both the A-Tile and B-Tile for each of the four array designs.

3.1.3 Edge Staple Modifications for Dynamic Fluorescence Monitoring

Two of the SEs on each active tile arm were designed with chemical modifications. One strand contains an internal Cy5TM fluorophore (648 nm excitation, 668 nm emission, reported) and the other is end terminated with an Iowa Black[®] RQ (500 to 700 nm

absorbance range, 656 nm peak absorbance, reported). The sticky-ends chosen for these modifications are such that the Cy5 modified strand on the A-Tile is complementary to the Iowa Black RQ strand on the B-Tile and when the two strands hybridize, the emission of the fluorophore is absorbed by the quencher and the observed fluorescence signal from the solution decreases. The separation of the dye and quencher on a single tile arm is large enough that tile arms cannot self-quench. Figure 3.3 shows the schematic for the active tile arms for the A-Tile and B-Tile, including the chemical modifications, both before and after hybridization of the two tile species.

A simple DNA duplex was designed to validate the quenching of the fluorescent signal when the chemically modified sticky-ends hybridize. Three oligonucleotides hybridize to form a double helix with an identical sequence to one of the chemically modified binding sites of the dimer. The duplex consists of the CO-A-R1-RQ quencher strand, an extended version of the CO-B-L1-Cy5 dye strand, and a CO-B-L1 complementary strand. The sequences of the complementary strand and the extension of the dye strand are such that they mimic the corresponding section of the scaffold strands in the origami cross-tiles to which the dye and quencher strands hybridize, as seen in Figure 3.5.

3.1.4 DNA Cross-Tile Synthesis

The A-Tile and B-Tile monomers were synthesized separately under identical conditions. M13mp18 scaffold strands and body and edge staple strands were mixed in a solution of 0.5X TBE and 12.5 mM MgCl₂ in a ratio of 5:10:1 body staples to edge staples to scaffold strands. The strands were annealed according the protocol outlined in Table A.4. Annealed tile solutions were gel purified in a 0.8% agarose gel prepared with

0.5X TBE, 8 mM MgCl₂ for 90 minutes at room temperature with a driving voltage of 70 V. Excess staple strands travel farther in the gel than well-formed origami structures which themselves travel farther than large DNA agglomerates. The origami band was extracted from the gel and squeezed between two glass slides to recover the DNA cross-tiles in an Eppendorf centrifuge tube. Origami structures were stored in the dark at room temperature in a solution of 0.5X TBE with 8 mM MgCl₂.

3.1.5 DNA Cross-Tile Concentration Measurement

DNA origami solution concentrations were determined by obtaining the absorbance of the solution at 260 nm and solving the Beer-Lambert Equation for concentration, c

$$c = \frac{A}{\epsilon \cdot b} \quad (1)$$

where A is the photon absorbance, b is the path length, and ϵ is the extinction coefficient for the origami structure. The origami extinction coefficient was calculated by the summation of the extinction coefficients for the dsDNA and ssDNA portions of the origami cross-tile with the extinction coefficients of the Cy5 fluorophores and Iowa Black RQ quenchers in each structure. Absorbance measurements were acquired using a NanoDrop One (Thermo Scientific), $b = 1$ cm, with the absorbance of 0.5X TBE with 8 mM MgCl₂ as a baseline. For each solution, an average of five measurements was used for the value of A in (1).

3.2 DNA Melting

Melting of the DNA origami cross-tile and array structure was monitored by measuring spectroscopic changes of the solution as temperature (T) was incrementally increased. Solutions were outgassed in a vacuum centrifuge for 20 minutes prior to melting experiments to prevent bubble formation in the samples at higher temperatures.

3.2.1 DNA Cross-Tile Melting

Melting of the DNA origami cross-tile was done in a Cary 5000 UV-Vis-IR Absorbance Spectrometer with a Peltier heater/cooler sample block in a Starna Cell Spectrophotometer Sub-Micro cuvette. The absorbance of a sample of 0.5X TBE, 8 mM MgCl₂ was used to establish a baseline measurement for the instrument prior to performing the melting. A gel-purified solution of the A-Tile ([MgCl₂] = 8 mM) was placed in the block and the temperature was increased from 20 °C to 80 °C at a rate of 0.1 °C/min while monitoring the absorbance of the solution at 260 nm.

3.2.2 Array Structure Melting

Melting of array structures was carried out in a Cary 5000 Agilent Fluorometer with a multi-cell Peltier heater/cooler block in a Starna Cell Fluorometer Sub-Micro cuvette. A-Tile and B-Tile solutions were mixed in equal concentrations (1 nM) and annealed at room temperature for at least 24 hours in 0.5X TBE, 8 mM MgCl₂ to allow the monomers to fully form arrays. The solution was then placed into the block at 10 °C for 30 minutes to allow the solution to reach equilibrium with the block temperature before beginning measurements. The block temperature was increased from 10 °C to 50 °C (60 °C for the unbounded array structures) at a rate of 0.1 °C/min while exciting the sample at 645 nm and monitoring the fluorescence signal at 670 nm. The fluorescence signal of A-Tile alone under identical conditions was collected to assess the signal response of the dye as a function of temperature.

3.3 Kinetics Measurements

Kinetic reaction rates were measured by monitoring the drop in the fluorescence over time of solutions containing dye strands and complementary quencher strands or of A-Tiles and B-Tiles at various temperatures and in different buffer conditions.

3.3.1 Temperature Dependent Kinetics Measurements

Temperature dependent kinetics measurements were performed with a Cary 5000 Agilent Fluorometer with a multi-cell Peltier heater/cooler block using tile solutions with $[\text{MgCl}_2] = 8 \text{ mM}$. Initial experimentation showed no significant difference in reaction rates between injecting B-Tile into A-Tile or vice versa. For optimal signal, the dye was excited at 650 nm and the emission was collected at 675 nm. 60 μL of A-Tile (or B-Tile) buffer solution was loaded into quartz fluorometer cuvettes (Starna, 16.40F-Q-10/Z15) and placed in the block along with the injecting solution 20 minutes prior to beginning data collection so that each could reach equilibrium temperature before the experiment began. A baseline fluorescence signal was acquired of the single A-Tile (B-Tile) solution before a small volume of higher concentration B-Tile (A-Tile) solution was injected into the cuvette at $t = 0$. The concentrations of A-Tile and B-Tile at $t = 0$ was $1 \pm 0.01 \text{ nM}$ for all reactions.

3.3.2 Magnesium Concentration Dependent Kinetics Measurements

Magnesium concentration dependent kinetics were performed with the block temperature holding at 20 °C and followed the same procedure as the temperature dependent kinetics measurements outlined above with a few notable differences. Baseline fluorescent measurements were collected immediately after loading the solution into the cuvette and the injecting solution was at equilibrium with lab ambient temperature (20

°C). MgCl_2 concentration of initial solutions were such that dilution upon injection brought the $[\text{MgCl}_2]$ to the desired level.

3.4 Atomic Force Microscopy

Samples were taken from solutions during kinetic experiments. Sample solutions were deposited on freshly cleaved mica and incubated for 4 minutes in a humid environment to discourage sample evaporation. Samples were then rinsed with filtered water and immediately dried with nitrogen (N_2) gas. AFM characterization was performed on a Bruker MultiMode 8 SPM with Nanoscope Controller in tapping mode using a silicon nitride probe (nominal tip radius of 2 nm). Post processing of AFM images was performed using WSxM Scanning Probe Microscopy Software⁴³.

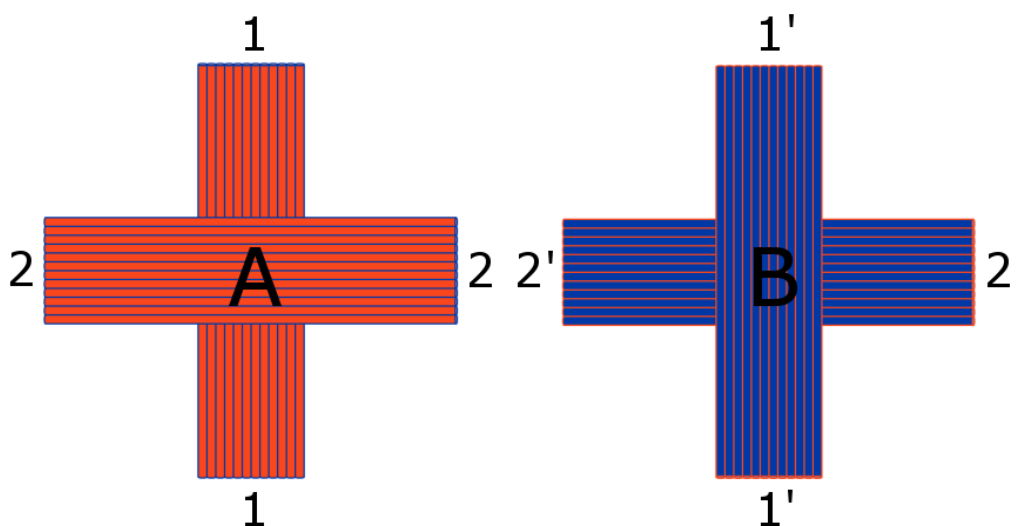


Figure 3.1. Diagram of A-Tile and B-Tile after folding. The B-Tile is oriented 90° clockwise relative to the A-Tile as defined by the hybridization interfaces 1, 2, 1', and 2'. The sticky-end sequences are designed so that 1 and 2 are complementary only to 1' and 2' respectively. This creates two-fold symmetry in the cross-tiles when all four tile arms are active.

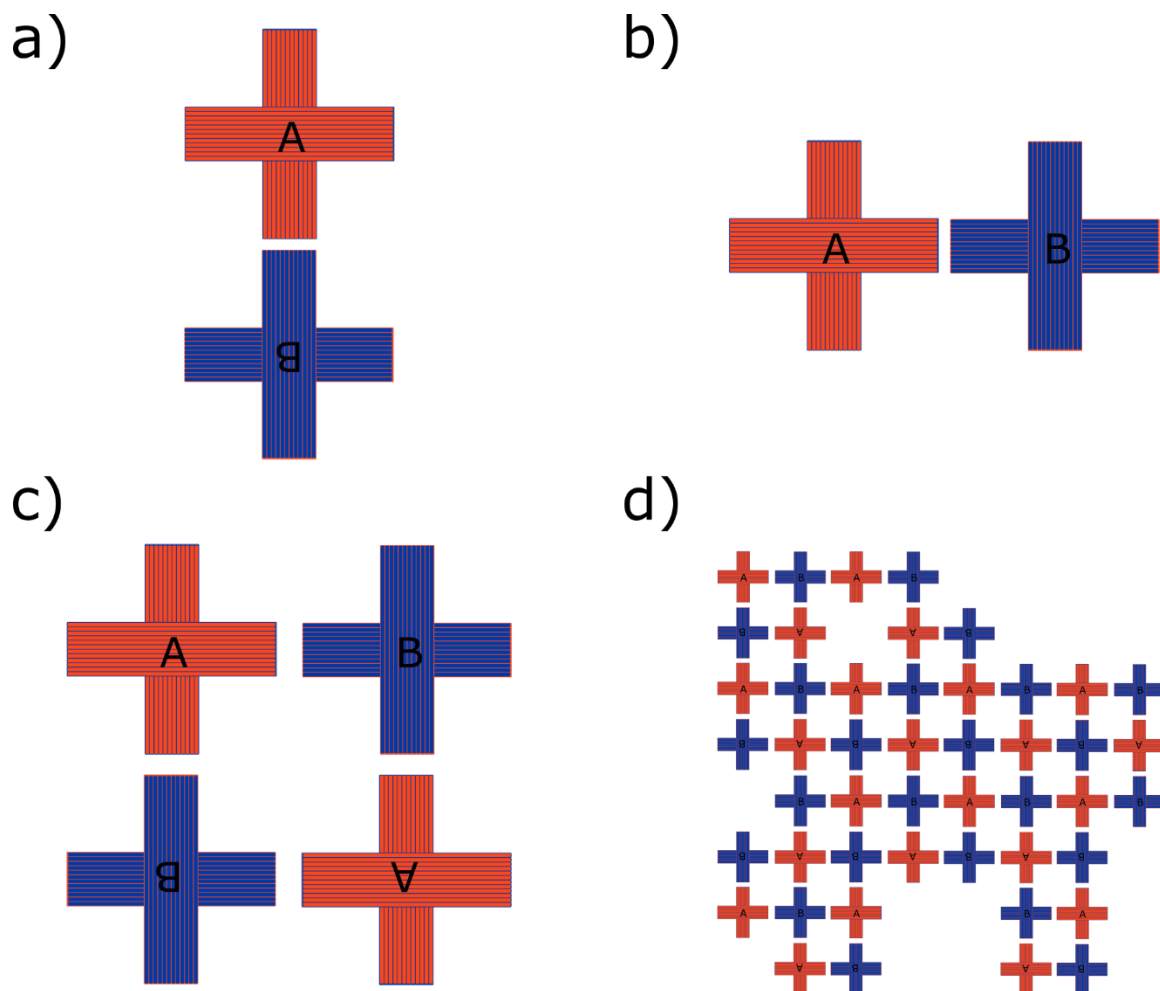


Figure 3.2. Schematics of the four array structures studied. (a, b) Activating one tile arm of either the 1-1' or 2-2' hybridization interfaces on each tile creates two unique dimer structures. (c) Activating one set of the 1-1' and 2-2' interfaces creates a 2x2 array. (d) Activating all four interfaces of each tile results in an unbounded array.

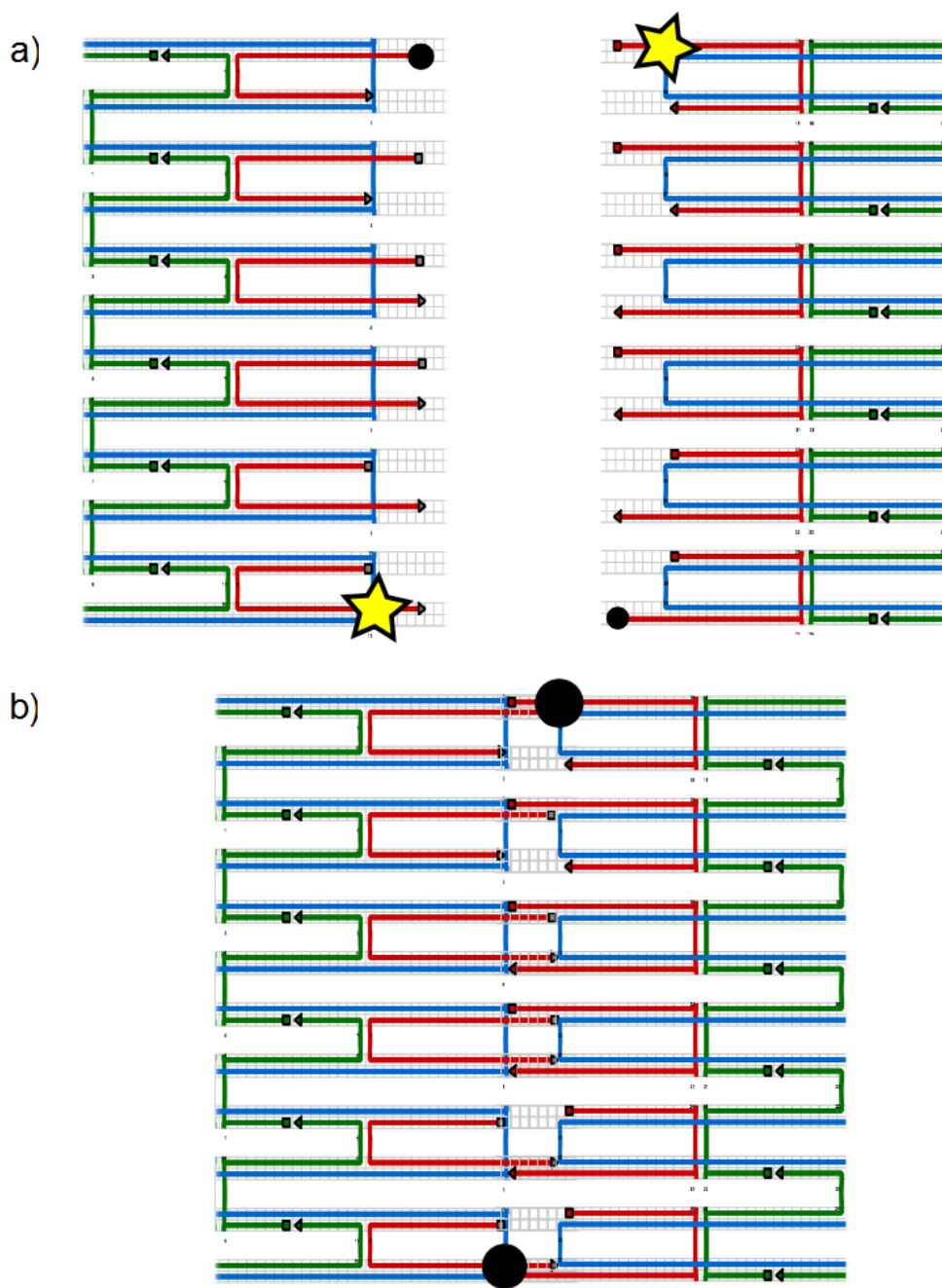


Figure 3.3. Schematic of a hybridization interface a) before and b) after hybridization. Two sticky-ends (red) on each tile arm are modified with either a fluorophore (gold star) or quencher (black circle). After hybridization, fluorescence from the tile arm is largely quenched which enables monitoring of array formation by fluorescence.

CHAPTER FOUR: RESULTS AND DISCUSSION

To gain a greater understanding of the underlying parameters of 2D DNA origami crystallization, simplified systems of origami cross-tile tiling structures were studied along with the unbounded array system. The modifications to the cross-tile design from Liu et al. described in the previous chapter limit the binding between tile species in a reaction to form one of the four array structures used in this study. Thermodynamic and kinetic parameters of these array structures were measured.

4.1 Validation of Design and Methods

To verify that the DNA strand hybridization between the A-Tile and B-Tile can be monitored by fluorescence quenching, and that this quenching assay is an accurate measure of structure formation, two proof-of-concept experiments were performed. First, a measurement of fluorescence over time for a dye labelled ssDNA and complimentary quencher labelled ssDNA reaction and second, a correlated AFM assay and fluorescence over time measurement of an $A+B \rightarrow AB$ dimer reaction.

4.1.1 Fluorescence Quenching of the Simple Duplex Hybridization

A solution of 5 nM CO-B-L1-Cy5-Ext dye strand and CO-B-L1-comp strand was prepared in 0.5X TBE, 8 mM MgCl₂ and given sufficient time to hybridize (>24 hrs). The hybridization of these two strands is not meant to affect the fluorescence of the Cy5 fluorophore on the dye modified strand but only to provide rigidity to the duplex. The fluorescent signal of the partially complete duplex was monitored for 5 minutes without observing a significant change in signal. At $t = 0$, a small volume of a high concentration

CO-A-R1-RQ quencher strand solution was injected into the dye/complementary strand solution bringing the final concentration of each component strand to 4.75 nM. An immediate drop in fluorescence signal was observed upon and as a consequence of injection. The decrease fluorescence over time for simple DNA duplex hybridization of $ssDNA_A + ssDNA_B \rightarrow dsDNA_{AB}$ can be modeled by the second-order kinetics rate law

$$F(t) = \frac{(F_{max} - F_{min}) \left(1 - \frac{[B]_0}{[A]_0}\right)}{1 - \frac{[B]_0}{[A]_0} e^{-k[A]_0 \left(1 - \frac{[B]_0}{[A]_0}\right)(t-t_0)}} + F_{min} \quad (2)$$

where F_{max} is the measured maximum fluorescence of the solution at injection, F_{min} is the final fluorescence, $[A]_0$ and $[B]_0$ are the initial concentrations of the ssDNA component strands at injection, k is the rate constant, and t_0 is the injection time of the second strand⁴⁴. Due to errors when pipetting, initial concentrations $[A]_0$ and $[B]_0$ are not equal in experimentation. Fitting the fluorescent data with this equation using k and F_{min} as fitting parameters and holding all other quantities fixed allows one to extract the effective reaction rate k_{on} . Applying this fit to the fluorescence data of the simple duplex hybridization at $[DNA] = 4.75 \pm 0.01$ nM gives us a value of $k_{on} = 1.43 \times 10^6$ M⁻¹s⁻¹ which is in agreement with published values for oligonucleotide hybridization reaction rates^{45, 46}. The data for the simple duplex hybridization and the fit of Equation (2) can be seen in Figure 4.1 and validates the spectroscopic method of monitoring DNA hybridization.

4.1.2 Fluorescent Signal Quenching as a Result of Dimer Formation

To confirm that the change in fluorescence signal in a solution of A-Tiles and B-Tiles is an adequate proxy for directly measuring the hybridization of tiles, a series of AFM samples were prepared from solution pulled from an ongoing dimer reaction while

simultaneously measuring the reaction kinetics. With only one species of cross-tile present in solution before injection of the complementary tile type, we see in Figure 4.2 (a) that the tiles exist almost entirely in monomer form indicating that tiles do not self-hybridize by design. Figure 4.2 (b) shows the tiles at injection, $t = 0$. We see that the two tile species are mostly present in monomer form as they have not had sufficient time to hybridize. We define the fluorescence at $t = 0$ as the maximum fluorescence (F_{\max}). The sample prepared at $t = 1500$ s (Figure 4.2 (c)) shows that 30% of the countable tiles have formed dimers while the fluorescence signal is $\sim 0.7 F_{\max}$. The final sample was prepared at $t < 14,000$ s after the majority of the reaction had progressed. As seen in Figure 4.2 (d), the percentage of tiles forming dimers is 70% of the countable tiles while the measured fluorescence is $\sim 0.3 F_{\max}$. The correlation between the percentage of F_{\max} at a certain time with the percentage of tiles that have hybridized at that time suggests that the method of using fluorescence signal as a proxy for monitoring hybridization is valid.

A small percentage of tiles were considered uncountable due to either their location at the edge of the image where all four arms were not in the field of view or because it was impossible to conclude if they were dimerized with a neighboring tile or not. The origami structures in the final AFM sample appear to be slightly degraded compared to the previous three samples. A number of factors could contribute to this, the quality of the mica cleave, the charge distribution on the surface, degradation of the origami from repeated pipette mixing while preparing samples, etc. It is important to note that in all of the atomic force micrographs captured, no structure comprised of more than two individual tiles was observed.

4.2 Thermodynamic Parameters of Array Structures and Monomers

Two separate spectroscopic approaches were utilized to perform melting curves of the individual cross-tile and of the origami dimer structures. From these curves, the melting temperature (T_m), enthalpy (ΔH°_{VH}), entropy (ΔS°), and energy of formation (ΔG°_T) were calculated. The melting temperature is defined as the temperature at which half of the base components of the system have disassociated from their natural state. For dimers, this is the temperature at which half of the initial dimer structures have separated into two individual tiles and for the individual cross-tile it is the temperature at which half of the staple strands have completely broken their base pair bonds and are free in solution. The melting temperature for an 2x2 cross-tile array is the temperature at which two of the four hybridization interfaces in the array have dissociated. Here we will define the melting temperature of an unbounded array as the temperature where half of the hybridization interfaces in the interior of the unbounded array have dissociated.

4.2.1 Determining Melting Temperature of DNA Origami Cross-Tile

The absorbance of 260 nm wavelength UV light of a solution of ssDNA is greater than that of the same solution where the DNA exists as dsDNA. For this reason, as staple strands begin to dissociate from the scaffold, the absorption of 260 nm light in the solution increases⁴⁷. Using the method outlined by Mergny et al. on the data collected from the melting experiment outlined in Section 3.2.1, upper and lower baselines for the absorbance_{260nm} versus temperature curve were produced by applying a linear fit to either extremes of the curve, shown in Figure 4.3⁴⁸. Using these two baselines, upper and lower endpoints for a median line were established by finding the midpoint between the lower baseline and upper baseline values at two temperature extremes, 0 °C and 90 °C in this

case. T_m is taken to be the point on the midline defined by these two endpoints which intersects the measured data. T_m for the origami cross-tile monomer is measured at 52.5 °C.

4.2.2 Melting Temperature of DNA Origami Array Structures

Fluorescence data from the melting experiment outlined in Section 3.2.2 showed an increase in signal for origami array solutions with increasing temperature. This increase is due to the separation of arrays into their component cross-tiles. Measuring the fluorescence of the A-Tile monomer solution vs T showed that the signal from the Cy5 modified dye strand is temperature dependent as seen in Figure 4.4 (a). A linear fit of the decrease in signal with increasing temperature allows one to correct for the decreasing dye signal by dividing the linear best fit line of the single tile fluorescence curve from the measured array data.

Figure 4.5 shows the corrected and analyzed melting curves for all four array structures. The measured melting temperatures are 31.6 °C and 33.6 °C for the 1-1' and 2-2' dimer respectively, 36.8 °C for the 2x2 array, and 45.8 °C for the UB array. In general, the melting temperatures increase with the number of active tile arms per monomer. From our four designs, we determined that the melting temperature increases 0.55 °C per active arm. This relationship suggests that hybridization interfaces work cooperatively with each other rather than independently. Both the 1-1' and 2-2' interfaces are identical in SE number and length but not in the sequences of component SEs. We observed a 2 °C difference in T_m between the 2-2' and 1-1' interfaces with the 2-2' interface being more thermally stable. In the case of the UB array structure, the lower linear region of the melting curve spans a temperature range from 10 °C to 35 °C. The

exact nature of this large linear area is presently unknown but may be a result of the dissociation of tiles on the exterior of arrays or out-of-plane hybridization defects which are bound by only one or two tile arms. Beyond 35 °C the curve follows a normal melting curve shape which may be described as the dissociation of all the interior tiles in a UB array.

4.2.3 Enthalpy, Entropy, and Gibb's Free Energy of Arrays

In addition to T_m , the components of the Gibb's free energy equation can be extracted from a melting curve. Using the method described by Marky and Breslauer, the van't Hoff enthalpy can be expressed as

$$\Delta H_{VH} = (2 + 2n)RT_m^2 \left(\frac{\delta\alpha}{dT} \right)_{T=T_m}, \quad (3)$$

where n is the molecularity of the reaction and α is the percentage of monomers in a hybridized state⁴⁹. The entropy can then be calculated from

$$\Delta S = \frac{\Delta H}{T_m} - R \ln\left(\frac{C_T}{4}\right), \quad (4)$$

where R is the universal gas constant and C_T is the cross-tile concentration. Using the Gibb's free energy equation,

$$\Delta G_T = \Delta H_{VH} - T\Delta S, \quad (5)$$

the energy of formation at a given temperature can be calculated for each of the four array structures. The molecularity of each reaction A-Tile + B-Tile = Array is $n = 2$. ΔG°_{293} of the 1-1' and 2-2' dimers were found to be -15.6 ± 0.8 and -15.7 ± 0.8 kcal mol⁻¹ respectively, consistent with published values for similar DNA hybridization interfaces^{28, 50}, and 17.2 ± 0.5 and -28.0 ± 1.3 kcal mol⁻¹ for the 2x2 and UB arrays. All of the calculated thermodynamic parameters are provided in Table 4.1.

4.3 Effects of Buffer Solution Conditions on Dimer Formation Rates

To gain an elementary understanding of the underlying kinetics of DNA cross-tile array formation, a number of reactions were monitored under various buffer conditions. Parameters of focus were buffer solution temperature and magnesium concentration. All kinetic experiments were performed in triplicate with the exception of the 50 mM [Mg] buffer reaction, which was only performed twice due to lack of adequate sample volume.

4.3.1 Temperature Dependence of Array Formation

A second order fit of the fluorescence data from the reaction A-Tile + B-Tile \rightarrow AB Array at various temperatures shows that k_{eff} is temperature dependent for all structures with an increasing reaction rate with increasing temperature. Figure 4.6 shows k_{eff} versus temperature for all four array structures. With the exception of the 2-2' dimer, we see a deviation from Arrhenius behavior in all the structures at higher temperatures. A possible explanation for the deviation from an Arrhenius relationship is the temperature dependence of k_{off} . In the case of the 1-1' dimer at 10 °C our calculated $\Delta G^{\circ}_{10\text{ }^{\circ}\text{C}} = -18.0$ kcal mol⁻¹ and the rate constant $K = \frac{k_{\text{on}}}{k_{\text{off}}} \times 1\text{ M} = e^{\left(\frac{-\Delta G^{\circ}}{RT}\right)} = 7.4 \times 10^{13}$. Assuming that $k_{\text{on}} \gg k_{\text{off}}$ then $k_{\text{eff}} \approx k_{\text{on}} = 1.7 \times 10^5 \text{ mol}^{-1} \text{ s}^{-1}$ and $k_{\text{off}} \approx 2.4 \times 10^{-9} \text{ s}^{-1}$. At 30 °C the off rate is $8.1 \times 10^{-5} \text{ s}^{-1}$. This 10^4 increase in k_{off} suggests that the reaction deviates from second order kinetics at higher temperatures. The departure from Arrhenius behavior in the two higher order structures suggests that the 1-1' hybridization interface is the rate-limiting step in array formation. Table 4.2 contains all the kinetic parameters measured and calculated for each of the four array structures. Values for the kinetic parameters of UB arrays are presented although the method used to calculate ΔG_T , and therefore K and k_{off} , is valid only under the assumption the reaction is a two-state process. The shape of

the melting curve suggests that this assumption may not hold in the case of the UB array and another method of calculating ΔG_T may be necessary.

4.3.2 Effect of Magnesium Concentration on Dimer Formation

The reaction rate of DNA cross-tile hybridization can be controlled by changing the concentration of magnesium in the buffer solution. The divalent salt cation acts to screen the negative charges of the origami structures and reduces the energy barrier to dimer formation. Figure 4.7 shows how k_{on} at 20 °C increases with increasing [Mg] and begins to saturate at around $4 \times 10^6 \text{ M}^{-1} \text{ s}^{-1}$. By modeling each origami cross-tile as an oblate spheroid in water with a long semi-axis of 50 nm (the length from the center of the tile to the edge of an arm) and short semi-axis of 1 nm (1/2 the thickness of the tile), one obtains for the diffusion coefficient of each cross-tile a value of $6.66 \times 10^{-12} \text{ m}^2/\text{s}$ at 20 °C⁵¹. This value is in agreement with published diffusion coefficients for DNA origami structures⁵²⁻⁵⁴. The diffusion limited reaction rate is represented by the dotted line in Figure 4.7 and is calculated by

$$k_{diffusion} = 4\pi(D_{Tile A} + D_{Tile B}) * R, \quad (6)$$

where D_{A-Tile} and D_{B-Tile} are the diffusion coefficients of A-Tile and B-Tile respectively and R is reaction volume. $k_{diffusion} = 1.66 \times 10^8 \text{ M}^{-1} \text{ s}^{-1}$. This high value indicates that the observed saturation of the reaction rate constant is related to sticky-end hybridization rather than diffusion.

4.4 Sedimentation of Unbound Arrays

Large 2D array formation is restricted by sedimentation of structures over time. The fluorescence during kinetic experiments with the unbound array structures exhibited an unusual increase in signal after three hours post injection. The increase in signal was

not a result of evaporation and AFM samples prepared after this amount of time were completely devoid of any DNA. To investigate this issue, the real space fluorescence of a well-mixed unbounded array solution was monitored over time. Figure 4.8 shows a time lapse of the fluorescence of solutions of individual cross-tiles, dimers, and unbound arrays. The unbound array sample showed significant precipitation of the DNA out of solution in only a few hours. None of the smaller structures displayed this sedimentation behavior during the same amount of time. The time scale of this sedimentation is much less than traditional array annealing protocols, which suggests that once arrays reach a certain size in stationary solutions, they will fall out of solution and may no longer have the ability to grow or anneal out defects. Figure 4.9 shows an AFM image of a sample taken from the bottom of a centrifuge tube containing a UB array solution. Previous samples prepared from the middle of this solution did not contain any observed tiles in AFM.

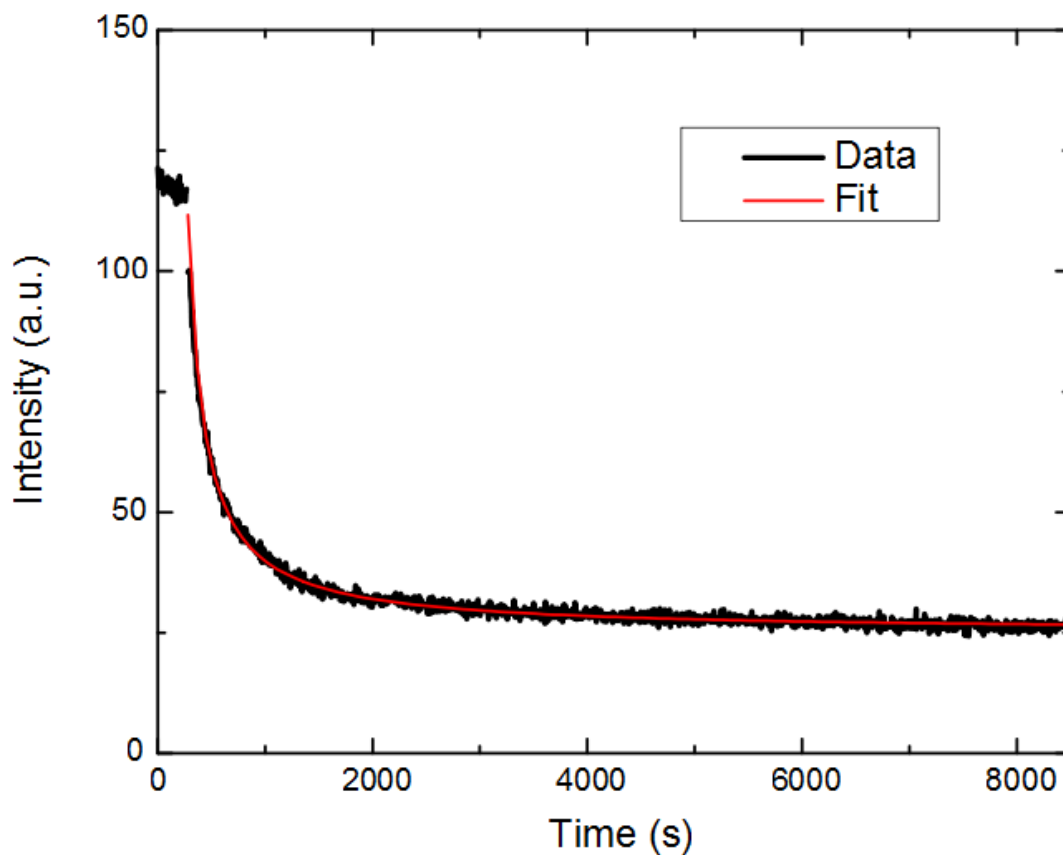


Figure 4.1. Fluorescence Intensity vs Time of a solution of CO-B-L1-Cy5-Ext dye strand and CO-B-L1-comp before and after the injection of the CO-A-R1-RQ strand. The initial fluorescence of the dye/complementary strand solution at $[DNA] = 5 \text{ nM}$ was measured for 300 seconds to establish a pre-injection fluorescence value. At $t = 300 \text{ s}$, the quencher strand was added to the solution, bringing the $[DNA]$ to 4.75 nM . Applying this dilution factor to the pre-injection fluorescence measurement provided an initial fluorescence parameter for our second order reaction fit. The calculated association rate for this simple duplex reaction is $k_{on} = 1.43 \times 10^6 \text{ M}^{-1}\text{s}^{-1}$.

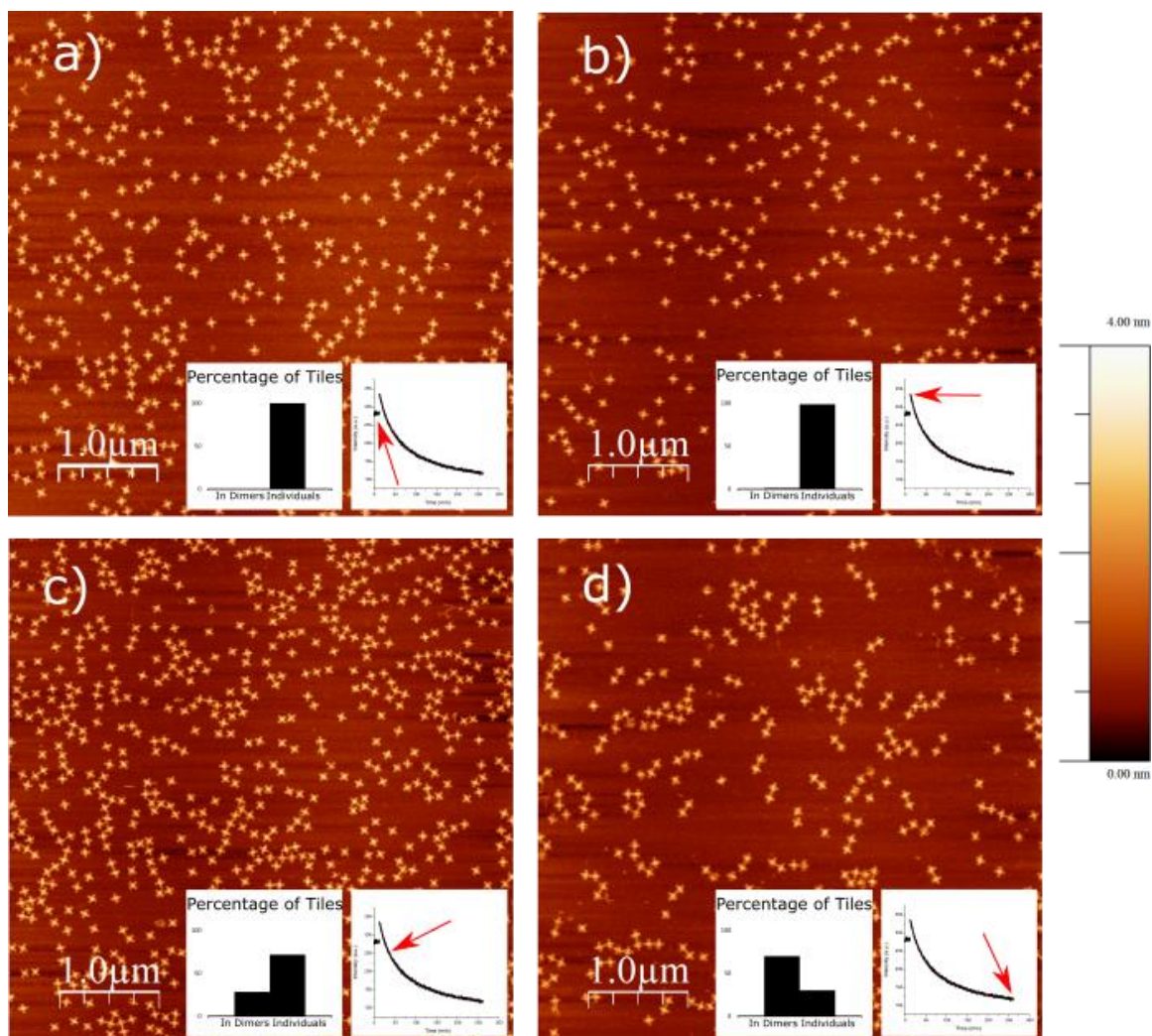


Figure 4.2. AFM images, the corresponding fluorescence value of the solution, and the count of cross-tiles as monomers and dimers of samples prepared at sequential time intervals (red arrows) from a 2-2' dimer formation reaction. a) Before injection only one tile species is present in solution. A pre-injection fluorescence value is measured at $[DNA] = 1 \text{ nM}$ and all the cross-tiles present in AFM exist as monomers. b) At injection ($t = 0$), the fluorescence of the solution with $[DNA] = 2 \text{ nM}$ has jumped due to the increase in the number of cross-tile monomers present. This fluorescence value is taken as the initial fluorescent parameter for the second order reaction fit. AFM shows that over 99% of the cross-tiles present exist in monomer form as there has been insufficient time for dimer formation to occur. c) At $t = 25$ minutes the total fluorescence of the solution has decreased to 70% of its initial value. Concurrently, AFM images show that ~30% of the cross-tiles have dimerized. d) At $t = 240$ minutes the total fluorescence has decreased to 30% of the initial value and 70% of the cross-tiles in AFM have dimerized.

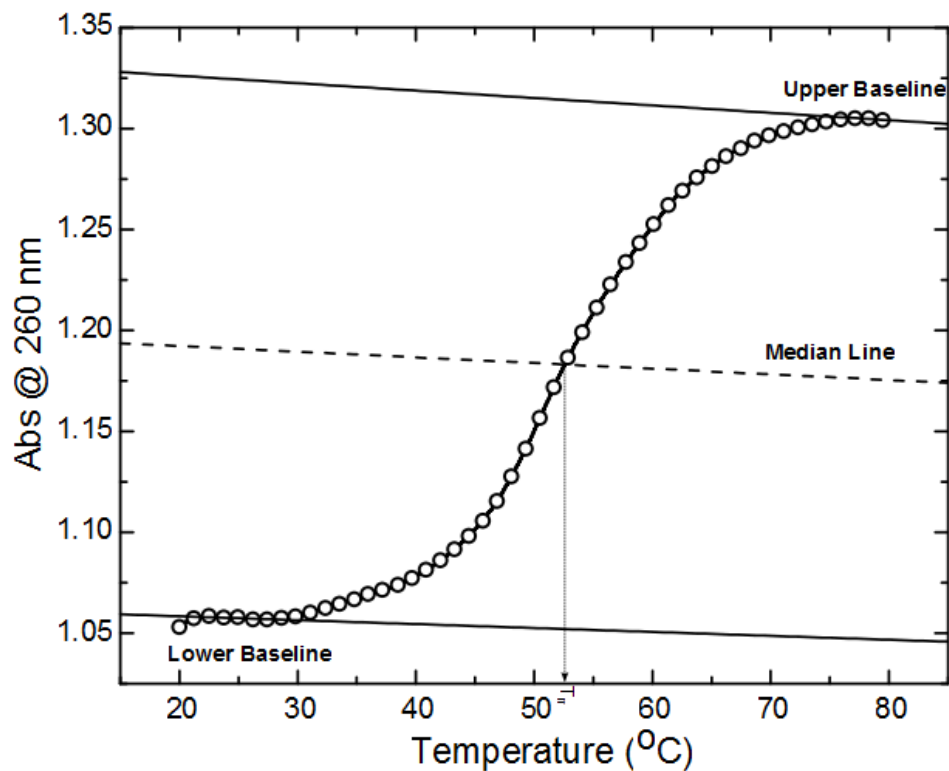


Figure 4.3. Cross-Tile Melting Curve. The absorbance of 260 nm light vs temperature of a 5 nM sample of A-Tile monomers. Upper and lower baseline equations are established from the linear regions of the curve at either temperature extremes. From the two baselines, a median line can be defined and T_m is defined as the temperature at which the median line crosses the measured data⁴⁸. The melting temperature of the A-Tile is measured at 52.5 °C. Since the B-Tile differs from the A-Tile by only 24 unique edge strands, this is taken to be the melting temperature of both monomers.

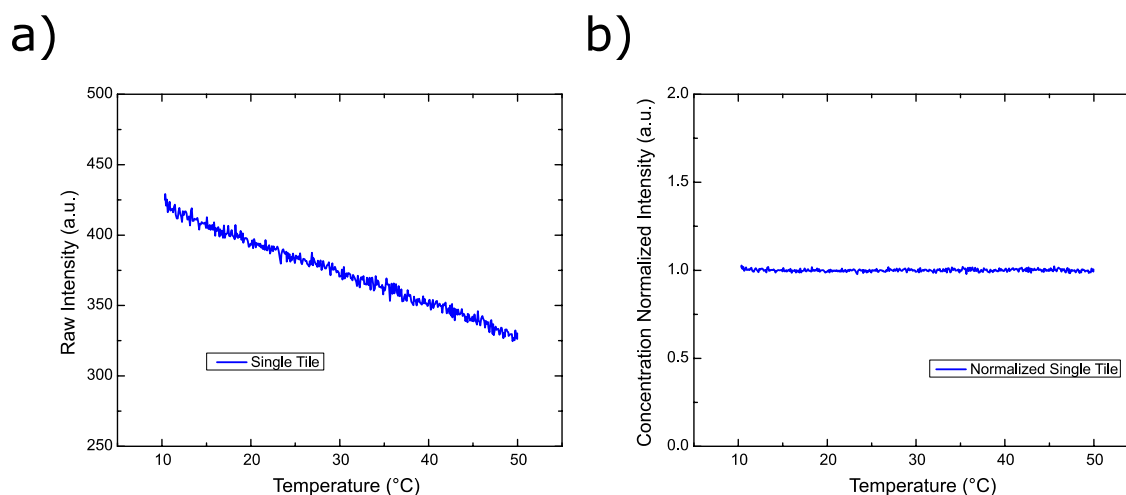


Figure 4.4. The effect of temperature on fluorescence of the dye strand on the cross-tile monomers. a) The raw melting curve data of an A-Tile monomer solution. The shape of the monomer solution curve indicates that as temperature increases, the base fluorescence signal of the dye labelled cross-tiles decreases. To correct for this effect, the linear fit line of the monomer curve was from the monomer. b) The resulting corrected melting curve accounting for the temperature dependence of the fluorescence signal. The monomer solution fluorescence is consistent over the entire temperature range. All array melting curves were normalized using this method with the linear fit lines coming from their own component single tiles.

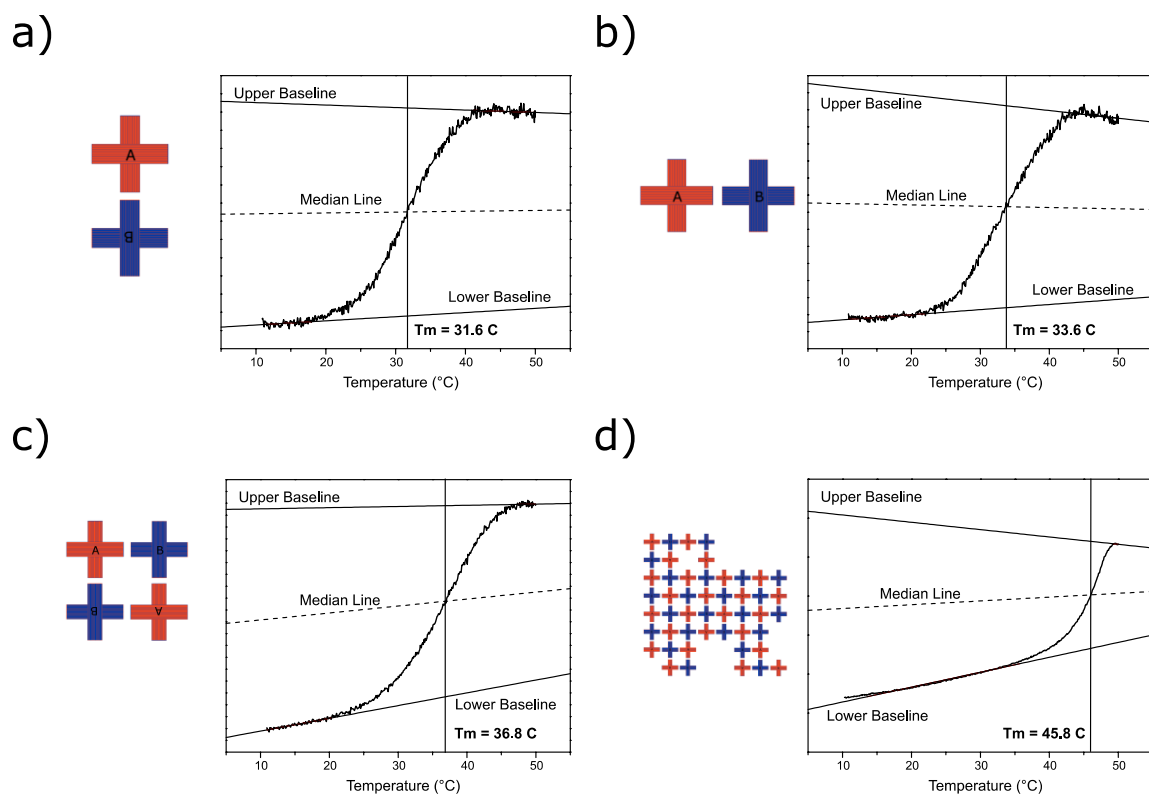


Figure 4.5. The schematics, melting temperatures, and analyzed temperature dependent fluorescence corrected melting curves for all a) the 1-1' dimer, b) the 2-2' dimer, c) 2x2 array, and d) the unbounded array structures. As the number of active tile arms per monomer increases, the melting temperature of the resultant array structures increases. Empirically, the increase in melting temperature is $0.56\text{ }^{\circ}\text{C}$ per sticky-end (8 sticky-ends per active tile arm).

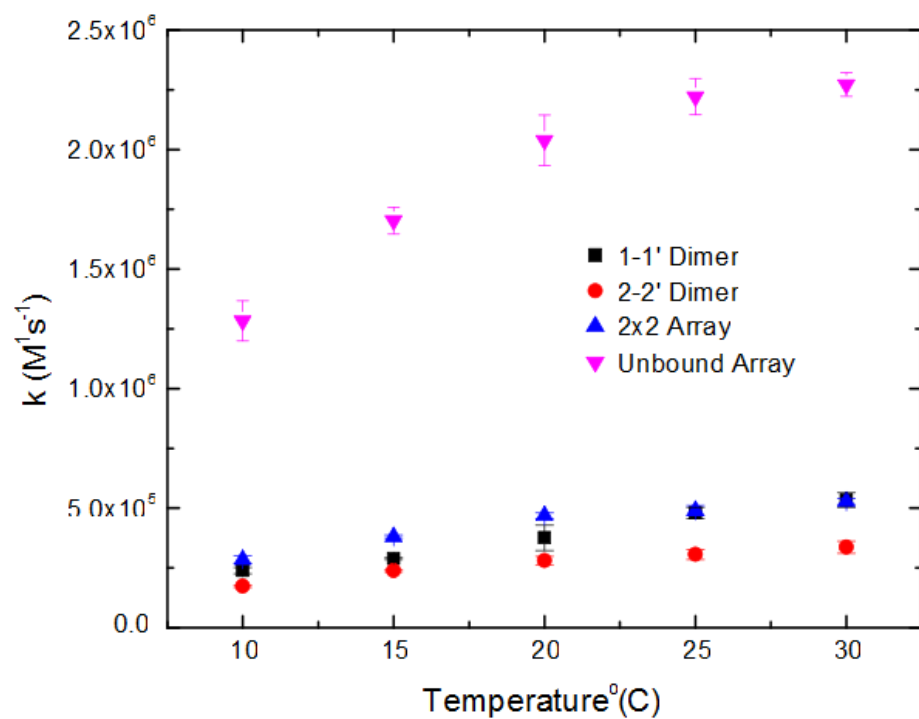


Figure 4.6. The measured association rates of the four structures as a function of temperature. In general, all the structures see an increase in association rate with increasing temperature. In addition, the association rate increases with an increase in active tile arms per monomer with the unbounded array showing a significant increase in association rate over the three restricted array size designs.

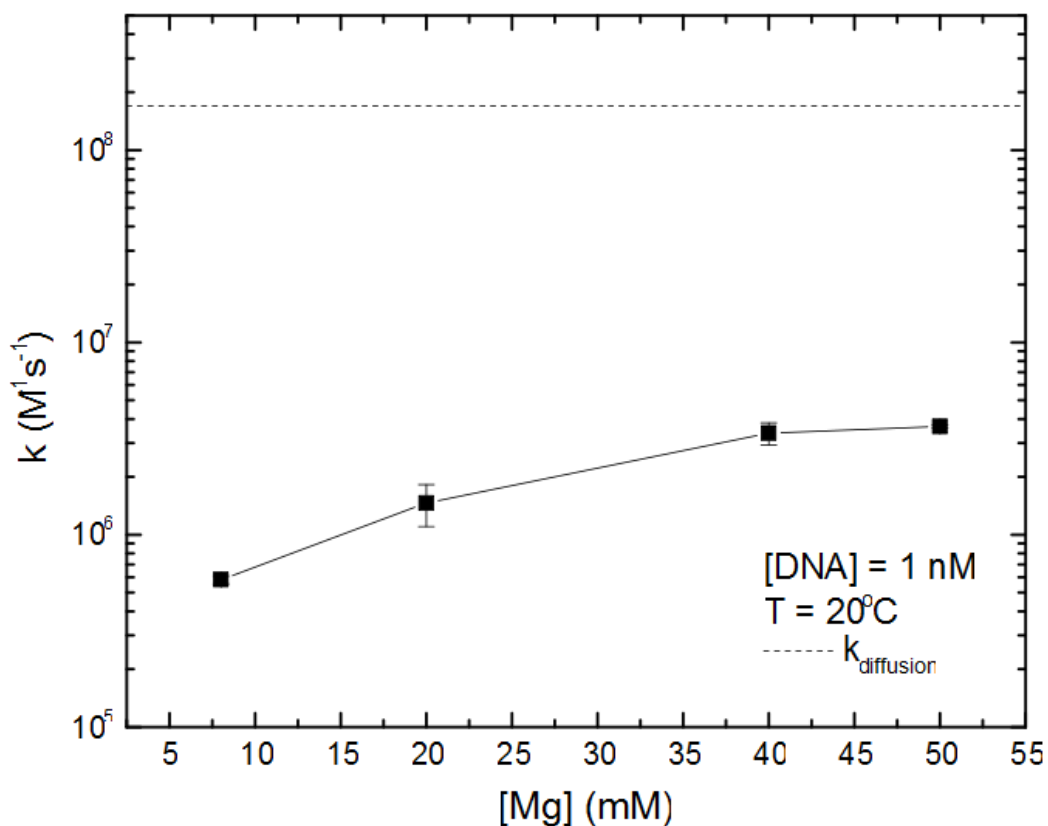


Figure 4.7. The buffer magnesium concentration dependence of the 2-2' dimer association rate. As the $[\text{Mg}^{++}]$ increases, the association rate increases as well. The association rate can be increased by nearly an order of magnitude with just over a six-fold increase in $[\text{Mg}^{++}]$. While the association rate can be significantly increased, it appears to saturate at $5 \times 10^6 \text{ M}^{-1} \text{ s}^{-1}$ which is still two orders of magnitude below the calculated diffusion limited association rate for these structures (dotted line).

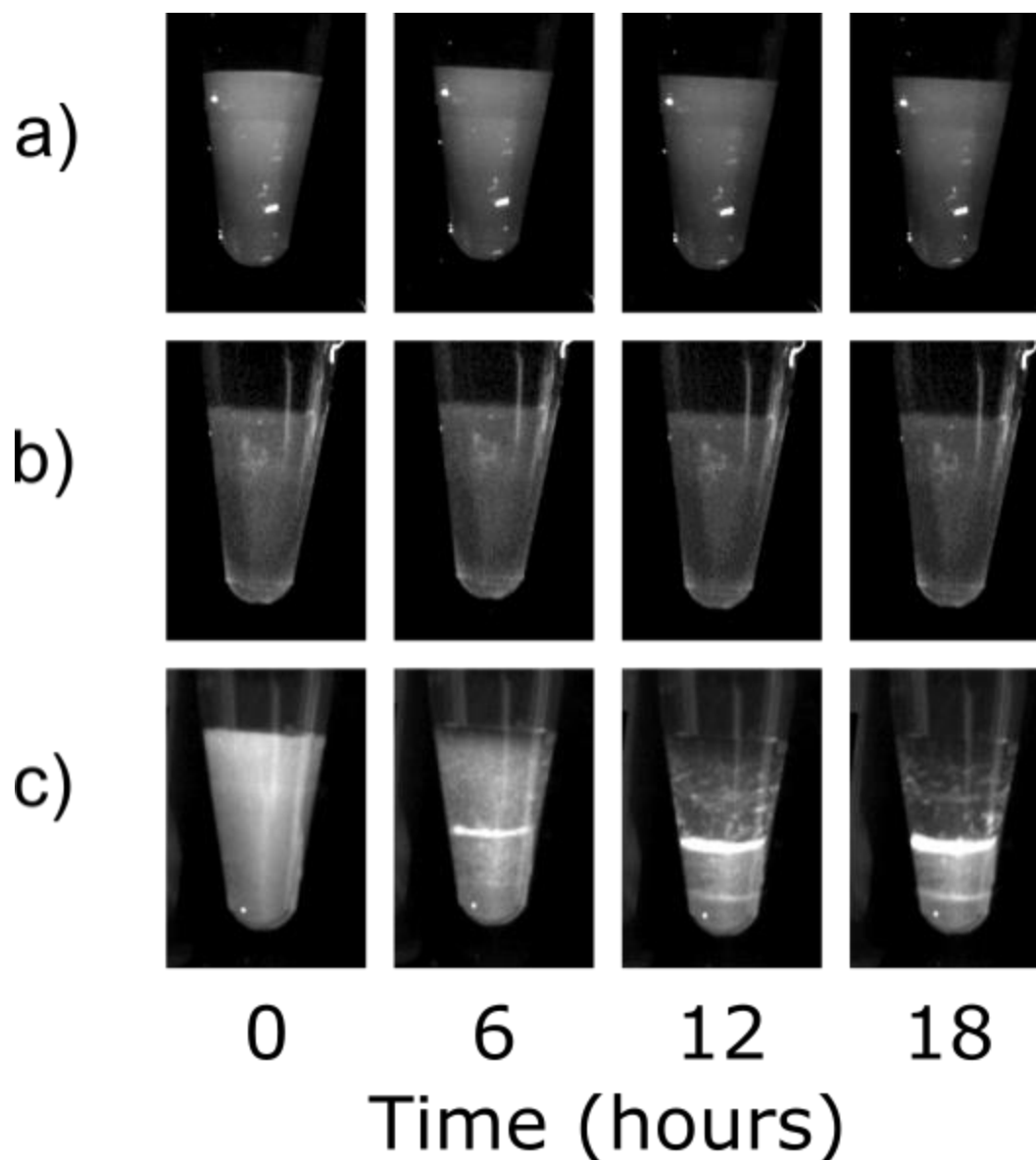


Figure 4.8. Time Lapse of the fluorescence of solutions containing (a) monomer cross-tiles, (b) 2-2' Dimers, and (c) unbound arrays. The monomers and smaller array structures remain suspended in solution for extended time periods but in the case of the unbound arrays, sedimentation of structures is observed in as little as six hours. At 12 hours, the top of the buffer solution is significantly depleted of structures and a second sedimentation ring has begun to form below the first. After 18 hours the upper portion of the solution contains almost no fluorescent origami structures as both sedimentation rings continue to grow.

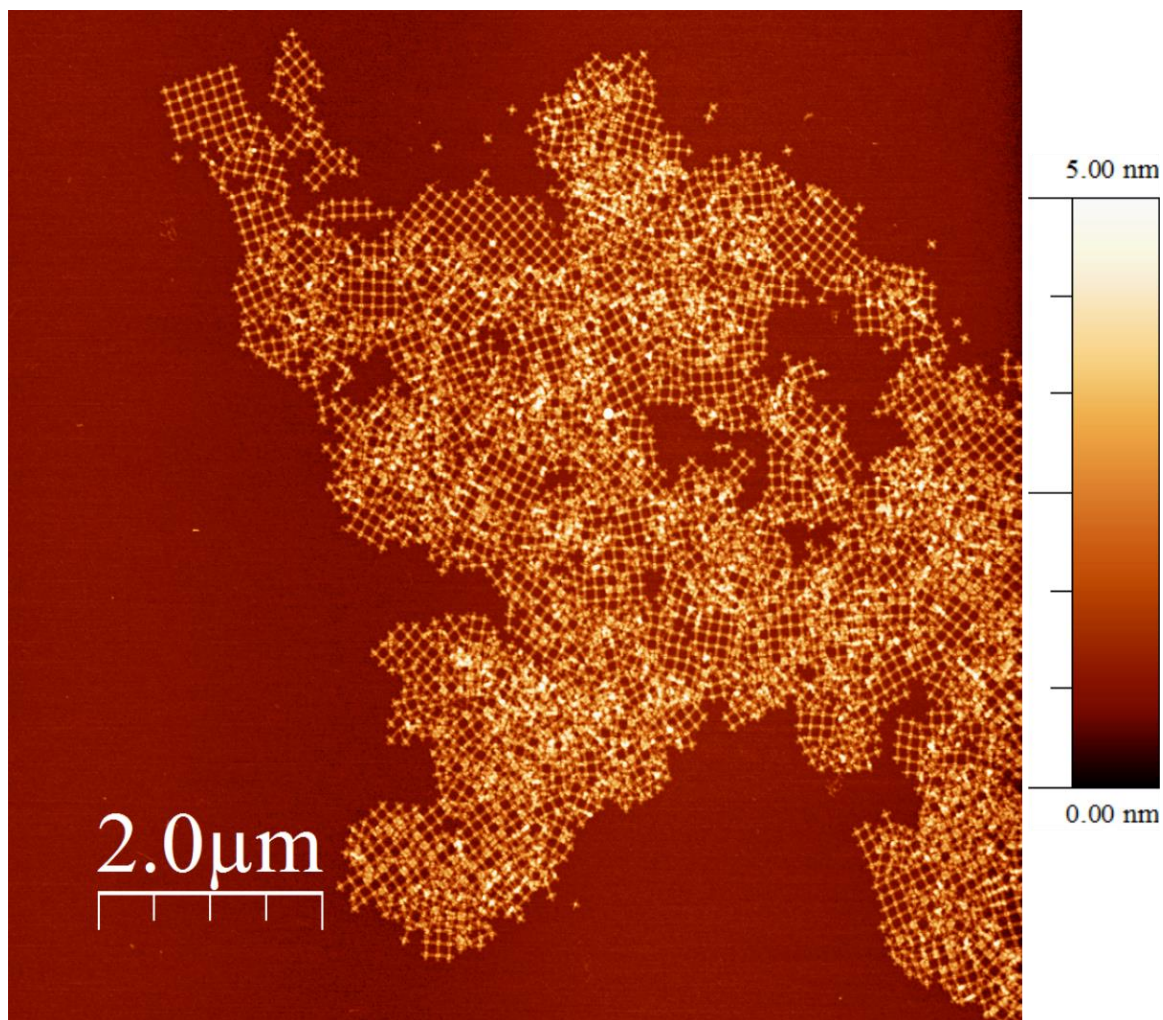


Figure 4.9. AFM image of structures in a sedimentation ring of an unbound array sample. The small domains of single-crystal origami cross-tile arrays in the polycrystalline aggregate suggest that the arrays reach some critical size before precipitating out of solution and creating areas of high local origami concentration. Arrays in these areas encounter each other at non-ideal angles and do not have enough mobility to undergo reorientation.

Table 4.1. Calculated Thermodynamic Parameters of Array Formation

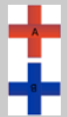
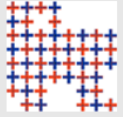
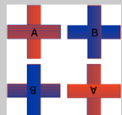
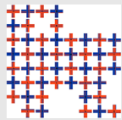
Structure	Name	Melting Temperature (°C)	ΔH_{vH} (kcal/mol)	$\Delta S \cdot 293 \text{ K}$ (kcal/mol)	$\Delta G @ 293 \text{ K}$ (kcal/mol)
	1-1' Dimer	31.6 ± 0.2	-83.4 ± 8.3	-67.7 ± 6.8	-15.6 ± 0.8
	2-2' Dimer	33.6 ± 0.2	-71.9 ± 7.2	-56.3 ± 5.6	-15.7 ± 0.8
	2x2 Array	36.8 ± 0.1	-87.7 ± 9.2	-70.5 ± 8.7	-17.2 ± 0.5
	UB Array	45.8 ± 0.2	-192.3 ± 17.7	-164.2 ± 16.4	-28.0 ± 1.3

Table 4.2. Measured and Calculated Kinetic Parameters of Array Formation

Structure	Name	Melting Temperature (°C)	K @ 30 °C	K _{on} @ 30 °C (M ⁻¹ s ⁻¹)	K _{off} @ 30 °C (s ⁻¹)
	1-1' Dimer	31.6 ± 0.2	4.68E+11	2.80E+05	5.99E-07
	2-2' Dimer	33.6 ± 0.2	4.80E+11	3.76E+05	7.83E-07
	2x2 Array	36.8 ± 0.1	6.96E+12	4.68E+05	6.73E-08
	UB Array	45.8 ± 0.2	8.26E+20	2.04E+06	2.47E-15

CHAPTER FIVE: CONCLUSIONS

Dimer formation is unlikely to occur at temperatures above 35 °C in buffer solutions with 8 mM [Mg⁺⁺]. At these temperatures, the kinetic energy of the system is great enough to break the 8x5 bp bonds between A-Tile and B-Tile. As temperatures increase to 52 °C and above, the individual cross-tiles disassociate into their component scaffold and staple strands. Establishing these critical temperatures is the first step in optimizing an annealing program to form large, defect free 2D DNA origami crystals.

When attempting to form large arrays in 8 mM [Mg⁺⁺], it is critical to avoid heating the solution above 52 °C as this will damage the individual tiles, possibly in a way that makes array formation improbable. At temperatures lower than 35 °C, tiles bound by only a single arm are stable in solution and each tile becomes a nucleation site. Growth of larger, low defect arrays in this condition is improbable. At temperatures near the unbounded array T_m, formation of nuclei will be slow as tiles bound by less than 4 arms will be unstable in solution.

The growth phase of 2D crystal formation may be accelerated by cyclic fluctuation of temperature between the critical temperatures of lower order array formation. While growth of arrays near the unbounded array melting temperature may occur with low defects, the process is kinetically slow. By lowering the temperature, binding events between fewer than 4 arms per tile are stable and growth will accelerate, although with the potential for more defects. After a period of time in this accelerated growth range, the temperature could be raised to near the unbounded array melting

temperature. This would cause tiles bound unfavorably to arrays to disassociate, leaving only low defect crystals in solution. Further study of nucleation and growth within this critical temperature range is necessary to establish robust protocols for cross-tile array formation.

Reaction rates can be controlled simply by adjusting buffer conditions. Previous work on DNA dimerization kinetics showed that reaction rates can be tuned by adjusting the length, rigidity, and number of linkers between origami structures²⁸. This method of control occurs in the design phase determines the baseline reaction rates for dimerization. For *in-situ* adjustment of reaction rates, varying the temperature and magnesium concentration of the buffer solution results in deviations from the baseline reaction rate determined by the design. Such dynamic control of reaction rates provides a useful control mechanism for forming large arrays, both in solution and through surface mediation. For example, during the nucleation phase of 2D crystal growth, it may be desirable to retard the rate of reaction so that a small number of nuclei are present and resulting arrays will have low poly-crystallinity. Once the reaction enters the growth phase, the rate can be increased to rapidly grow single domain 2D arrays and eventually suppressed to control array size. A greater understanding of how higher order structures respond to changes in buffer conditions is needed to fully understand unrestricted 2D DNA origami crystal formation. Future work on investigating DNA origami cross-tile dimerization includes studying the effects of buffer pH and monovalent cation concentration on reaction rates.

REFERENCES

1. K. Galatsis, K. L. Wang, M. Ozkan, C. S. Ozkan, Y. Huang, J. P. Chang, H. G. Monbouquette, Y. Chen, P. Nealey and Y. Botros, *Advanced Materials*, 2010, **22**, 769-778.
2. R. A. Segalman, *Materials Science and Engineering: R: Reports*, 2005, **48**, 191-226.
3. M. Neisser and S. Wurm, *Advanced Optical Technologies*, 2015, **4**, 235.
4. V. Mishra, G. H. Fredrickson and E. J. Kramer, *ACS Nano*, 2012, **6**, 2629-2641.
5. S. M. Douglas, A. H. Marblestone, S. Teerapittayanon, A. Vazquez, G. M. Church and W. M. Shih, *Nucleic Acids Research*, 2009, **37**, 5001-5006.
6. H. Bui, C. Onodera, C. Kidwell, Y. Tan, E. Graugnard, W. Kuang, J. Lee, W. B. Knowlton, B. Yurke and W. L. Hughes, *Nano Letters*, 2010, **10**, 3367-3372.
7. B. Ding, Z. Deng, H. Yan, S. Cabrini, R. N. Zuckermann and J. Bokor, *Journal of the American Chemical Society*, **2010**, **132**, 3248-3249.
8. S. Pal, Z. Deng, B. Ding, H. Yan and Y. Liu, *Angewandte Chemie*, 2010, **122**, 2760-2764.
9. W. P. Klein, C. N. Schmidt, B. Rapp, S. Takabayashi, W. B. Knowlton, J. Lee, B. Yurke, W. L. Hughes, E. Graugnard and W. Kuang, *Nano Letters*, 2013, **13**, 3850-3856.
10. S. Takabayashi, W. P. Klein, C. Onodera, B. Rapp, J. Flores-Estrada, E. Lindau, L. Snowball, J. T. Sam, J. E. Padilla, J. Lee, W. B. Knowlton, E. Graugnard, B. Yurke, W. Kuang and W. L. Hughes, *Nanoscale*, 2014, **6**, 13928-13938.
11. X. Shen, C. Song, J. Wang, D. Shi, Z. Wang, N. Liu and B. Ding, *Journal of the American Chemical Society*, 2012, **134**, 146-149.
12. A. S. Kuzyk, R. Fan, Zhiyuan Pardatscher, G. Roller, E.-M. Hoge, A. Simmel, F. C. Govorov, A. O. Liedl and T. Liedl, *Nature*, 2012, **483**, 311-314.
13. X. Lan and Q. Wang, *NPG Asia Mater*, 2014, **6**, e97.
14. R. Schreiber, J. Do, E.-M. Roller, T. Zhang, V. J. Schuller, P. C. Nickels, J. Feldmann and T. Liedl, *Nat Nano*, 2014, **9**, 74-78.
15. M. Langecker, V. Arnaut, T. G. Martin, J. List, S. Renner, M. Mayer, H. Dietz and F. C. Simmel, *Science*, 2012, **338**, 932-936.
16. Q. Zhang, Q. Jiang, N. Li, L. Dai, Q. Liu, L. Song, J. Wang, Y. Li, J. Tian, B. Ding and Y. Du, *ACS Nano*, 2014, **8**, 6633-6643.
17. W. Liu, H. Zhong, R. Wang and N. C. Seeman, *Angewandte Chemie International Edition*, 2011, **50**, 264-267.
18. R. Jungmann, M. Scheible, A. Kuzyk, G. Pardatscher, E. C. Carlos and F. C. Simmel, *Nanotechnology*, 2011, **22**, 275301.

19. T. C. Wu, M. Rahman and M. L. Norton, *Accounts of Chemical Research*, 2014, **47**, 1750-1758.
20. C. G. Evans, R. F. Hariadi and E. Winfree, *Journal of the American Chemical Society*, 2012, **134**, 10485-10492.
21. A. Aghebat Rafat, T. Pirzer, M. B. Scheible, A. Kostina and F. C. Simmel, *Angewandte Chemie International Edition*, 2014, **53**, 7665-7668.
22. S. Woo and P. W. K. Rothmund, *Nat Commun*, 2014, **5**.
23. G. Tikhomirov, P. Petersen and L. Qian, *Nature Nanotechnology*, 2016, **12**, 251.
24. C. M. Green, K. Schutt, N. Morris, R. M. Zadegan, W. L. Hughes, W. Kuang and E. Graugnard, *Nanoscale*, 2017, **9**, 10205-10211.
25. H. G. Hansma and D. E. Laney, *Biophysical Journal*, 1996, **70**, 1933-1939.
26. S. Hamada and S. Murata, *Angewandte Chemie International Edition*, 2009, **48**, 6820-6823.
27. A. R. Chandrasekaran and R. Zhuo, *Applied Materials Today*, 2016, **2**, 7-16.
28. J. Zenk, C. Tuntivate and R. Schulman, *Journal of the American Chemical Society*, 2016, **138**, 3346-3354.
29. C. Lin, Y. Liu, S. Rinker and H. Yan, *ChemPhysChem*, 2006, **7**, 1641-1647.
30. C. G. Evans and E. Winfree, *Chemical Society Reviews*, 2017, **46**, 3808-3829.
31. H. Zhang, J. Chao, D. Pan, H. Liu, Q. Huang and C. Fan, *Chemical Communications*, 2012, **48**, 6405-6407.
32. N. C. Seeman, *Journal of Theoretical Biology*, 1982, **99**, 237-247.
33. N. R. Kallenbach, R.-I. Ma and N. C. Seeman, *Nature*, 1983, **305**, 829-831.
34. T. J. Fu and N. C. Seeman, *Biochemistry*, 1993, **32**, 3211-3220.
35. X. Li, X. Yang, J. Qi and N. C. Seeman, *Journal of the American Chemical Society*, 1996, **118**, 6131-6140.
36. Y. Ke, Y. Liu, J. Zhang and H. Yan, *Journal of the American Chemical Society*, 2006, **128**, 4414-4421.
37. Y. Ke, L. L. Ong, W. M. Shih and P. Yin, *Science*, 2012, **338**, 1177.
38. P. W. K. Rothmund, *Nature*, 2006, **440**, 297-302.
39. A. V. Pinheiro, D. Han, W. M. Shih and H. Yan, *Nat Nano*, 2011, **6**, 763-772.
40. Z. Zhao, Y. Liu and H. Yan, *Nano Letters*, 2011, **11**, 2997-3002.
41. F. Zhang, J. Nangreave, Y. Liu and H. Yan, *Journal of the American Chemical Society*, 2014, **136**, 11198-11211.
42. S. Jiang, F. Hong, H. Hu, H. Yan and Y. Liu, *ACS Nano*, 2017, **11**, 9370-9381.
43. I. Horcas, R. Fernández, J. M. Gómez-Rodríguez, J. Colchero, J. Gómez-Herrero and A. M. Baro, *Review of Scientific Instruments*, 2007, **78**, 013705.
44. E. Graugnard, D. L. Kellis, H. Bui, S. Barnes, W. Kuang, J. Lee, W. L. Hughes, W. B. Knowlton and B. Yurke, *Nano Letters*, 2012, **12**, 2117-2122.
45. L. E. Morrison and L. M. Stols, *Biochemistry*, 1993, **32**, 3095-3104.
46. D. Y. Zhang and E. Winfree, *Journal of the American Chemical Society*, 2009, **131**, 17303-17314.
47. J. SantaLucia, in *Spectrophotometry and Spectrofluorometry. A Practical Approach*, ed. M. G. Gore, Oxford University Press, 2nd edn., 2000, pp. 329-356.
48. J.-L. Mergny and L. Lacroix, *Oligonucleotides*, 2004, **13**, 515-537.
49. L. A. Marky and K. J. Breslauer, *Biopolymers*, 1987, **26**, 1601-1620.
50. R. F. Hariadi, B. Yurke and E. Winfree, *Chemical Science*, 2015, **6**, 2252-2267.

51. R. F. Probstein, *Physicochemical hydrodynamics: an introduction*, John Wiley & Sons, 2005.
52. A. Czogalla, E. P. Petrov, D. J. Kauert, V. Uzunova, Y. Zhang, R. Seidel and P. Schuille, *Faraday Discussions*, 2013, **161**, 31-43.
53. K. Du, S. H. Ko, G. M. Gallatin, H. P. Yoon, J. Alexander Liddle and A. J. Berglund, *Chemical Communications*, 2013, **49**, 907-909.
54. L. Gan, T.-C. Chao, F. Camacho-Alanis and A. Ros, *Analytical Chemistry*, 2013, **85**, 11427-11434.

APPENDIX A

DNA Origami Cross-Tile and DNA Duplex Designs

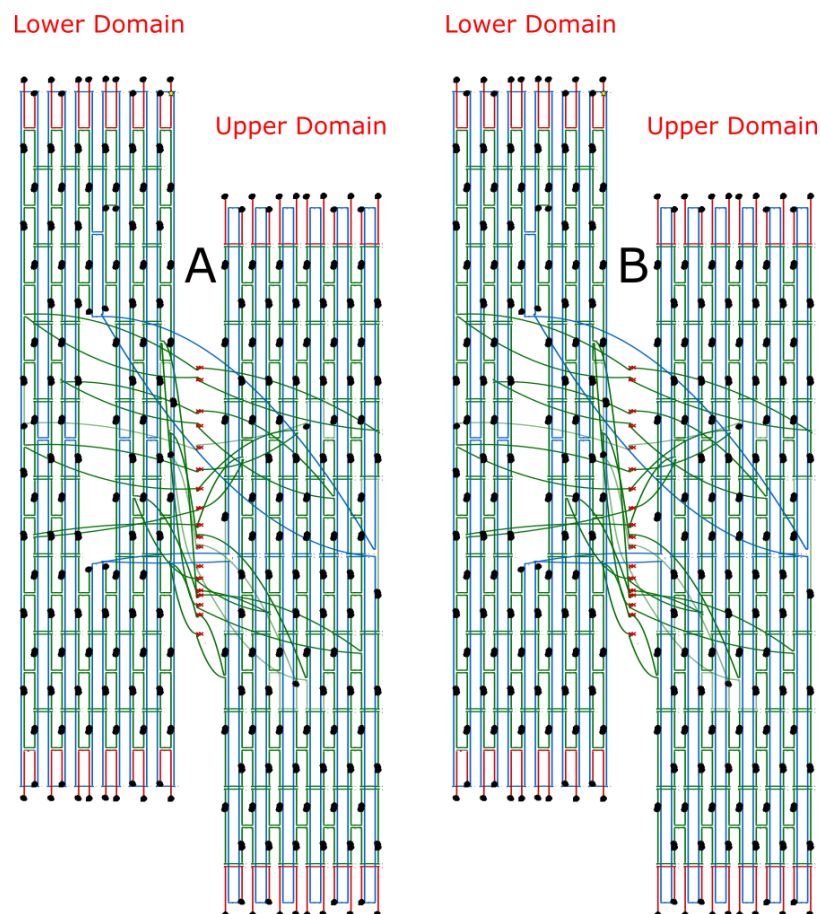


Figure A.1. Design schematic of DNA cross-tiles (A, B) from caDNAno. The two helical portion (Upper, Lower) of each cross-tile are achieved by rastering the single stranded m13mp18 scaffold strand (blue) parallel to the long axis of each domain. Short staple body stands (green) bind to specific sections of the scaffold strand to fold the scaffold and pin it in place. Staple strands in the middle of the cross-tile (denoted by red 'xx') bind to both helical domains in such a way that the two domains are held perpendicular to each other. Edge staple strands (red) have eight five base-pair single strands, sticky-ends, extending from the cross-tile arms.

APPENDIX B

Kinetics Reaction Curves and 2nd Order Rate Fits

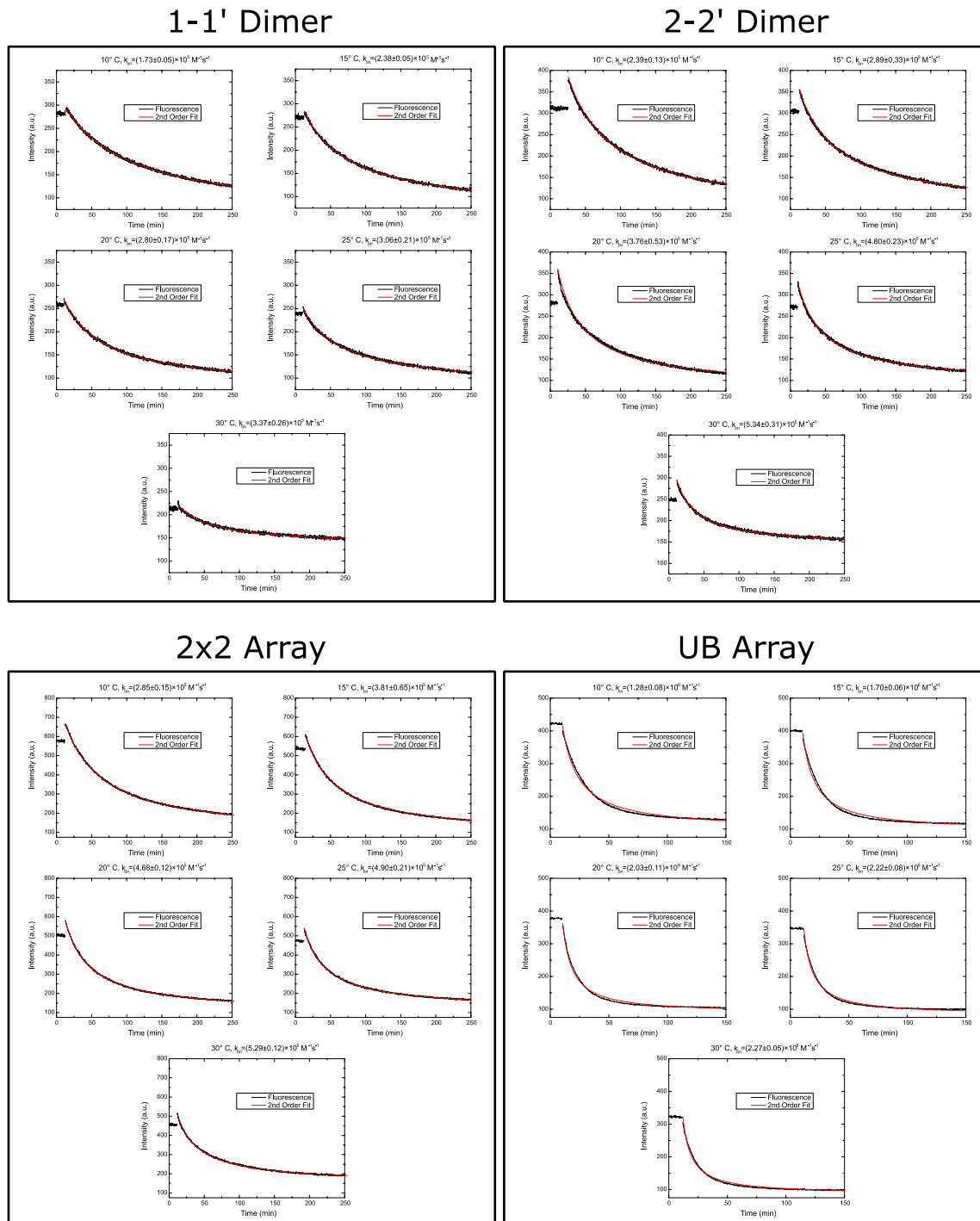


Figure A.3. Kinetic measurements (black line) and the 2nd order kinetic rate fit (red line) for each of the four array structures at 10 °C, 15 °C, 20 °C, 25 °C, and 30 °C. The R^2 values for all fits are > 0.98.

APPENDIX C

DNA Origami Cross-Tile Staple Lists

Table A.1. Cross Tile Body Staple Sequences

<i>Name</i>	<i>Sequence</i>
CO-M-1	AGCTAATGCAGAACGCGCCTGTTTTAATATCC
CO-M-2	CATCCTAATTTGAAGCCTTAAATCTTTTATCC
CO-M-3	TGAATCTTGAGAGATAACCCACAAAACAATGA
CO-M-4	AATAGCAATAGATGGGCGCATCGTACCGTATC
CO-M-5	GGCCTCAGCTTGCATGCCTGCAGGGAATTCGT
CO-M-6	AATCATGGTGGTTTTCTTTTCACCCGCCTGG
CO-M-7	CCCTGAGAGAGTTGCAGCAAGCGGGTATTGGG
CO-M-8	CGCCAGGGTCATAGCTGTTTCCTGGACGGCCA
CO-M-9 [c]	GTGCCAAGGAAGATCGCACTCCAGATAGGTCA
CO-M-10	CGTTGGTGTAGCTATCTTACCGAATTGAGCGC
CO-M-11 [c]	TAATATCAACCAACGCTAACGAGCCCGACTTG
CO-M-12	CGGGAGGTTTTACGAGCATGTAGAACATGTTC
CO-M-13	CTGTCCAGACGACGACAATAAACAAACCAATC
CO-M-14	AATAATCGCGTTTTAGCGAACCTCGTCTTTCC
CO-M-15	AGAGCCTACAAAGTCAGAGGGTAAGCCCTTTT
CO-M-16	TAAGAAAAGATTGACCGTAATGGGCCAGCTTT
CO-M-17	CCGGCACCCACGACGTTGTAAAAGTGTGAAAT
CO-M-18	TGTTATCCGGGAGAGGCGGTTTGCTCCACGCT
CO-M-19	GGTTTGCCCCAGCAGGCGAAAATCAATCGGCC
CO-M-20	AACGCGCGGCTCACAATTCCACACCCAGGGTT
CO-M-21	TCCCAGTGCTTCTGGTGCCGGAAGTGGGAAC
CO-M-22	AAACGGCGGTAAGCAGATAGCCGAAACTGAAC
CO-M-23	ACCCTGAAATTTGCCAGTTACAAATTCTAAGA
CO-M-24	ACGCGAGGGCTGTCTTTCCTTATCAAGTAATT
CO-M-25	AATATAAAGTACCGACAAAAGGTAATTCCAAG
CO-M-26	AACGGGTAGAAAGGCTTATCCGGTAATAAACAG
CO-M-27	CCATATTAATTAGACGGGAGAATTACAAAGTTACC
CO-M-28	GTCGGATTCTCCACCAGGCA
CO-M-29	AAGCGCAATTAAGTTGGGTAACGAACATACG
CO-M-31	CCTGTCGTGCATAAAGTGTAAGCGATGTGCT
CO-M-32	GCAAGGCGTTTCGCCATTCAGGCTGCGCAACTG
CO-M-33	GGAAGCGCTTTATCCCAATCCAAAAGCAAAT
CO-M-35	AGGCATTTTCGAGCCAGTACTCATCG
CO-M-36	AGAACAAGTACCGCGCCCAATAGCTAAGAAAC
CO-M-37	GATTTTTTACAGAGAGAATAACATAAAAACAG
CO-M-39	CCTAATGAACTGCCGCTTTCCAGCCCTTATA
CO-M-42	TTGCGCTCGTGAGCTAACTCACATGATAGCCC
CO-M-43	TATTACGCGCGATCGGTGCGGGCGAGGATTT
CO-M-44	CAGCCTTTGTTAACGTCAAAAATTTTCAATT
CO-M-45	GGAATCATCAAGCCGTTTTTATTTGTTATATA

CO-M-47 ACTATATGCTCCGGCTTAGGTTGGTCATCGTA
CO-M-48 ACCTGAGCAGAGGCGAATTATTCAGAAAATAG
CO-M-49 AGAAGTATAATAGATAATACATTTCTCTTCGC
CO-M-50 TAAACATCTTTAATGCGCGAACTTAATTGCG
CO-M-51 CTATTAGTCGCCATTA AAAATACCATAGATTA
CO-M-52 GAGCCGTCTAGACTTTACAAACAATTGACAA
CO-M-54 TTTTAACTAAATGCTGATGCAAATTGAGAA
CO-M-56 CAAGACAAAATCATAGGTCTGAGACAAACAT
CO-M-57 CAAGAAAAATTGCTTTGAATACCAAGTTACAA
CO-M-58 CTCGTATTGGTGCCTAACA ACTAGAACGAAC
CO-M-60 TGCTGGTAATATCCAGAACAATATAAGCGTAA
CO-M-61 GAATACGTGAAGATAAAACAGAGGATCTAAAA
CO-M-62 TATCTTTAAAATCCTTTGCCCGAACCGCGACCTGC
CO-M-63 CGAAACAAAGTAATAACGGA
CO-M-64 TTCGCCTGCAAATTAATTACATTAATAGTGA
CO-M-66 ATATGCGTTATACAAATTCTTACCTTTTCAA
CO-M-67 TATATTTTGACGCTGAGAAGAGTCTAACAATT
CO-M-68 TGATTTGATACATCGGGAGAAACACAACGGAG
CO-M-70 ATTTTAAAGGAATTGAGGAAGGTTTGAGGCGG
CO-M-71 TCAGTATTAACCCTTCTGACCTGATACCGCCA
CO-M-72 GCCATTGCAACAGGAAAAACGCTCTGGCCAAC
CO-M-73 [c] AGAGATAGAACACCGCCTGCAACAAAATCAAC
CO-M-74 AGTAGAAAAGTTTGAGTAACATTA
CO-M-76 GTACCTTTATTACCTTTTTTAATGCGATAGCT
CO-M-77 [c] TAGATTAAGTTAATTTTCATCTTCTTAGTATC
CO-M-78 TCATAATTACTAGAAAAAGCCTGTTGACCTAA
CO-M-79 ATTTAATGATCCTTGAAAACATAGGAAACAGT
CO-M-80 ACATAAATACGTCAGATGAATATATGGAAGGA
CO-M-81 [c] TTAGAACCAATATAATCCTGATTGTCATTTTG
CO-M-82 CGGAACAATATCTGGTCAGTTGGCGTGCCACG
CO-M-83 CTGAGAGCAATAAAAAGGGACATTCATGGAAAT
CO-M-84 [c] ACCTACATTTTGACGCTCAATCGTCAGTCACA
CO-M-85 CGACCAGTCAGCAGCAAATGAAAATCAAACCC
CO-M-86 TCAATCAAAGAAACCACCAGAAGGATGATGGC
CO-M-87 AATTCATCAACCATATCAAATTATAGATTTT
CO-M-88 CAGGTTTACAATATATGTGAGTGATTAATTTT
CO-M-89 CCCTTAGAGTTTGAATACCGACCCACCGGAA
CO-M-90 ATAAGCAAAAATTCGCGTTAAATTTTTGTTAA
CO-M-91 CTCATATAAAAGATTCAAAGGGTAAGATTGT
CO-M-92 CGAACGAGAAATGGTCAATAACCTTTAGAACC
CO-M-93 ATAGTCAGGGAAGCCCGAAAGACTCAATTCTG
CO-M-94 ACCACATTTTACGAGGCATAGTAATGACTATT
CO-M-95 [c] CAAGAGTAATCAACGTAACAAAGCTTAGGAAT
CO-M-96 [c] CAGTGAATGCGCATAGGCTGGCTGACCTTCAT

CO-M-97 [c] CTATCATAATTCATCAGTTGAGATTGCTCATT
CO-M-98 CGCGTTTTAATCAGGTCTTTACCCGAGCAACA
CO-M-99 ATATTTTCTGTAACAGTTGATTCTCAAATAT
CO-M-100 CCGGAGACGCAAGGATAAAAATTTGTTTAGCT
CO-M-101 ATCAGCTCAAGCCCCAAAAACAGGGAGAAAGG
CO-M-102 AATCAGAAATTTTTTAACCAATAGGAACGCCA
CO-M-103 ATTTCAACAGTCAAATCACCATCACGGTTGAT
CO-M-104 TCATTCCAATTTGGGGCGCGAGCTAAGCCTTT
CO-M-105 AAATCAAAAATTCGAGCTTCAAAGTGGAAGTT
CO-M-106 GTAGAAAGACCCTCGTTTACCAGAATGACCAT
CO-M-107 [c] CAGACCAGAAGGCTTGCCCTGACGTATTACAG
CO-M-108 CAGAACGAGAAAGAGGACAGATGAACGGTGTA
CO-M-109 [c] AAAACCAAATAACGGAACAACATAGAAACAC
CO-M-110 [c] ACCGGAAGAGTTCAGAAAACGAGACGACGATA
CO-M-111 GGCATCAAATAAAGTACGGTGTCCGAACCAG
CO-M-112 TTCAACCGAATACTTTTGCGGGAGGAAAAGGT
CO-M-113 TCAAAAATTCAATCATATGTACCCATATGATA
CO-M-115 GACCCTGTTTCTAGCTGATAAATTTTCGTA
CO-M-116 AACAGTTAACCAGAGCCGCCCAGAACCGCC
CO-M-118 TAAAACGAAATAGCGAGAGGCTTTCTCAAATG
CO-M-119 CCAACTTTGTAGTAAATTGGGCTTTACGTTAA
CO-M-121 AGAGTACCTATTCATTGAATCCCCTGCAAAG
CO-M-122 [c] CATCCAATAATGCTGTAGCTCAACATGTTT
CO-M-123 AGAGGGTAAATCGGTTGTACCAAAGCATTAA
CO-M-124 CCAGCTTTAATCGATGAACGGTAAAATGCCGG
CO-M-125 AACAAGAGCATCAACATTAATGTGAGCGAGTAACAACTTAAGGAAACCGAGGAAA
CO-M-127 GTCATAAATTTAATTGCTCCTTTTCTTAATTG
CO-M-128 GTCAGGACCCAGAGGGGGTAATAGGCGGAATC
CO-M-129 AACGAGGCGCAGACGGAACCTTAAATCATTGTGTTATACCA
CO-M-130 GCGCCGACTTTAAGAACTGGCTCAAATTACCT
CO-M-131 CAACGCCTGATAGCGTCCAATACTTAAAATGT
CO-M-132 TATTATTCTGCGGATGGCTTAGAGGATAAGAG
CO-M-133 CCTCAGAGATTAAGCAATAAAGCCGCAAAGAA
CO-M-134 CGTCACCGGTCATTGCCTGAGAGTCTACAAAG
CO-M-135 GCTATCAGACTTGAGCCATTTGGGATTATCAC
CO-M-136 TTAGCAAACCACCACCTCAGAGCACCGCCAC
CO-M-137 GTCATTTTTGAAACATGAAAGTATTCGGAACC
CO-M-138 TTAGACTGGTAGCATTCCACAGACACAAACTA
CO-M-139 TATGCGATAATGACAACAACCATCCGATAGTT
CO-M-140 ATAACCGATCATCTTTGACCCCCAGCGATTATACCAAGTTCATGTTACTTAGCCGG
CO-M-142 GAACCACCATGCCCCCTGCCTATTTAAGAGGC
CO-M-143 CCAGCAAAAGCCGCCACCCTCAGACGCCACCA
CO-M-144 CGCAATAATAACGGAATATTCATTAAGGTGAAATTAGAG
CO-M-146 GTAACACTCTCAAGAGAAGGATTAGGATTA

CO-M-147 AGAATTTTCGTAACGATCTAAAGTTCATGTACC
 CO-M-148 TAAACACTATATTCGGTTCGCTGATTTTCGAGG
 CO-M-150 TTTCCAGACGGTTTATCAGCTTGC GGCTTGCA
 CO-M-152 AGCAAGGCACCAGAGCCACCACCGGCATTGAC
 CO-M-153 AGACTCCTTTGAGGGAGGGAAGTTTACCATT
 CO-M-154 TCAACCGATATTACGCAGTATGTTAGCAAACG
 CO-M-155 TCACCGGACGGAAACGTCACCAATGGCGACAT
 CO-M-156 GGGTCAGTGAGGCAGGTCAGACGAAATCAAAA
 CO-M-157 GGGATAGCGCTCAGTACCAGGCGGTTTTAACG
 CO-M-158 AATTGTATCGTTAGTAAATGAATTCATTTTCA
 CO-M-159 CAACCTAAAAGGCCGCTTTTTCGGGAGCCTT
 CO-M-160 CCCTCAGCTACGTAATGCCACTACGAAGGCAC
 CO-M-161 GGGATTTTAAAAGGCTCCAAAAGGATCGTCA
 CO-M-162 CGTCGAGATCAGAGCCACCACCTTTCTGTAT
 CO-M-163 GATATTCAGTGTACTGGTAATAAGATAAGTGC
 CO-M-164 CGATAGCATTGCCATCTTTTCATTTGGCCTT
 CO-M-165 TAGAAAATGCGCCAAAGACAAAAGGAAACCAT
 CO-M-166 GTTTACCAACATACATAAAGGTGGCAACATAT
 CO-M-167 TATTAGCGGCACCGTAATCAGTAGTTCATATG
 CO-M-168 [c] ATACAGGACAAACAAATAAATCCTAGCCCCCT
 CO-M-169 CGCCACCCGGGTTGATATAAGTATTTTTGATG
 CO-M-170 TCTCCAAAGCTAAACAACCTTCAACTCAGAAC
 CO-M-171 GGGTAAAAAGCGAAAGACAGCATCGTTGAAAA
 CO-M-172 GGTAGCAATTCATGAGGAAGTTTCCATTAAAC
 CO-M-173 GCGGAGTGATAATAATTTTTTACGGAACGAG
 CO-M-174 ATAGGTGTCCTCAGAACCGCCACCCAGTTTCA
 CO-M-175 CCAGAATGAAGCGTCATACATGGCAGCCCGGA
 CO-M-176 TCAAGTTTCGGCATTTCGGTCATCATTAAAG
 CO-M-177 AAAAGAAACACAATCAATAGAAAACGACAGAA
 CO-M-30*(1) AGCCGGAAGCCAGCTGCATTAATGCTGTTTGATGGTGTCTTCCTGTAG
 CO-M-114*(1) CTAGCATGAATTCGCGTCTGGCTGTTCCGAAATCGGCAAATTCGGGAAA
 CO-M-38*(2) TTGGGAAGCAGCTGGCTTAAAGCTAGCTATTTTGGAGAGATCTGGAGCA
 CO-M-126*(2) CTGAATCTAAATCATACAGGCAAGTCAGAGCATGAAAGGGGCTGGGGTG
 CO-M-40*(3) AATCAAAAGAATAGCCCTTTAAATATGCATTCTACTAATAGTAGTAACATTAT
 CO-M-41*(3) GAGATAGGGTTGTCAGGATTAG
 CO-M-117*(3) CTTTAAACCAAACCTCCAACAGTTGAGTGTGTTTCGTAGAAGAACTCAAACCTTTGAATGG
 CO-M-59*(4) CACCAGCAGGCACAGATTTAATTTCTCAATCATAAGGGAAACCGAACTGA
 CO-M-120*(4) AAGTTTTGGTTGGGAAGAAAATCGAGATGGTTCAATATTTATCGGCCT
 CO-M-53*(5) AATCGCGCAAAGAAGTTAGTTAGCTTAAACAGCTTGATACGCCACGC
 CO-M-141*(5) TGAGACTCGAGTTTCGTACCAGTAGCCCTCATATGATGAAAGACTACC
 CO-M-65*(6) ATTTATCAAGAACGCGAGAAAAGTATAAAGCCAATAAAGAATACAC
 CO-M-149*(6) GGGAGTTAAACGAAAGAGGCGTCAACAGTAGGGCTTATCCAATCG
 CO-M-55*(7) TCGCCATATTTAAACAACGTTGCGGGGTTTTAAGCCCAATAGGAACCTTGTGCTC
 CO-M-46*(7) [c] CCAACATGTTGTGCCGTATA

<i>CO-M-151*(7)</i>	AGGAGGTTGCCTTGAGTAACATAATTTAGGCAG
<i>CO-M-34*(8)</i>	CAGATATATTAACCATACGGAAATTACCCAAAAGAACTGGCATGATTA
<i>CO-M-145*(8)</i>	TCCCTCAGATCACCAGTAGCACCAAAATATTGTAGTACCGCAATAAGAG
<i>CO-M-69#</i>	TTTGGATTATACCTGATAAATTGTGTGCGAAATCGTTATTA
<i>CO-M-75#</i>	ATTTGTATCATCGCTTCTGAATTACAGTAACA

Table A.2. 1-1 Dimer A-Tile Edge Staple Sequences

Name	Sequence
<i>CO-A-R1-6T</i>	TTTTTTGTTAAATAAGAATAAAAGTGTGATAAATAAGGC
<i>CO-A-R2-6T</i>	TTTTTTAAATCGTCGCTATTAATAACCTTGCTTCTGT
<i>CO-A-R3-6T</i>	TTTTTTAAATAAAGAAATTGCGTTAGCACGTAAAACAGTTTTTT
<i>CO-A-R4-6T</i>	TTTTTTATTCTGATTATCAGAGCGGAATTATCATCATTTTTT
<i>CO-A-R5-6T</i>	TGCTGAACCTCAAATAATCTAAAGCATCACCTTTTTTT
<i>CO-A-R6-6T</i>	ACATTGGCAGATTCACCTGAAATGGATTATTTTTTTTT
<i>CO-A-D1-Cy5</i>	CGTAA/iCy5/CGTTAATATTTTGTTAATATTTAAATTGTAAA
<i>CO-A-D2</i>	GACATTGAGTAATGTGTAGGTTTTTAAATGCAATGCC
<i>CO-A-D3</i>	CTATCATTAGATACATTTTCGCTAGATTTAGTTTGACCACTTG
<i>CO-A-D4</i>	TGAGTATCAAAAAGATTAAGAAAAGCAAAGCGGATTGCTCTAC
<i>CO-A-D5</i>	ATAACGCCAAAAGGAACAATAATGCAGATACGTTCA
<i>CO-A-D6-RQ</i>	GGATATTCATTACCCAATCTTCGACAAGAACCAGTGT/3IAbRQSp/
<i>CO-A-L1-6T</i>	TCCTGAACAAGAAAAAATCAACAATAGATAAGTTTTT
<i>CO-A-L2-6T</i>	TTGCACCCAGCTACAAAAGATTAGTTGCTATTTTTTTT
<i>CO-A-L3-6T</i>	TTTTTTAATAATAAGAGCAAGAGAATTGAGTTAAGCCCTTTTTT
<i>CO-A-L4-6T</i>	TTTTTTGTTTGAGGGGACGACGAACCGTGCATCTGCCATTTTTT
<i>CO-A-L5-6T</i>	TTTTTTCCCGGTACCGAGGTCTCGACTCTAGAGGATC
<i>CO-A-L6-6T</i>	TTTTTTAGCTGATTGCCCTTCACAGTGAGACGGGCAAC
<i>CO-A-U1-6T</i>	AATAAGTTTATTTTGTGCGCAAAGACACCACGGTTTTTT
<i>CO-A-U2-6T</i>	TGTAGCGGTTTTTCATGCCTTTAGCGTCAGACTTTTTT
<i>CO-A-U3-6T</i>	TTTTTTAATTTACCGTTCCAGTGAAAGCGCAGTCTCTGTTTTTT
<i>CO-A-U4-6T</i>	TTTTTTGGTTTAGTACCGCCACATCACCGTACTCAGGATTTTTT
<i>CO-A-U5-6T</i>	TTTTTTACTAAAGGAATTGCGAAGAATAGAAAGGAACA
<i>CO-A-U6-6T</i>	TTTTTTGAGGACTAAAGACTTTCGGCTACAGAGGCTTT

Table A.3. 1-1 Dimer B-Tile Edge Staple Sequences

Name	Sequence
<i>CO-B-L1-6T</i>	TTTTTCGTTAATATTTTGTTAATATTTAAATTGTAAA
<i>CO-B-L2-6T</i>	TTTTTTGAGTAATGTGTAGGTTTTTAAATGCAATGCC
<i>CO-B-L3-6T</i>	TTTTTTATTAGATACATTTTCGCTAGATTTAGTTTGACCTTTTTT
<i>CO-B-L4-6T</i>	TTTTTTATCAAAAAGATTAAGAAAGCAAAGCGGATTGCTTTTTT
<i>CO-B-L5-6T</i>	ATAACGCCAAAAGGAACAACCTAATGCAGATACTTTTTT
<i>CO-B-L6-6T</i>	GGATATTCATTACCCAATCTTCGACAAGAACCTTTTTT
<i>CO-B-U1-6T</i>	TCCTGAACAAGAAAAAATCAACAATAGATAAGTTTTT
<i>CO-B-U2-6T</i>	TTGCACCCAGCTACAAAAGATTAGTTGCTATTTTTTTTT
<i>CO-B-U3-6T</i>	TTTTTTAATAATAAGAGCAAGAGAATTGAGTTAAGCCCTTTTTT
<i>CO-B-U4-6T</i>	TTTTTTGTTTGAGGGGACGACGAACCGTGCATCTGCCATTTTTT
<i>CO-B-U5-6T</i>	TTTTTTCCCGGTACCGAGGTCTCGACTCTAGAGGATC
<i>CO-B-U6-6T</i>	TTTTTTAGCTGATTGCCCTTTCACAGTGAGACGGGCAAC
<i>CO-B-R1-6T</i>	AATAAGTTTATTTTGTGCAAAGACACCACGGTTTTTTT
<i>CO-B-R2-6T</i>	TGTAGCGCGTTTTTCATGCCTTTAGCGTCAGACTTTTTT
<i>CO-B-R3-6T</i>	TTTTTTAATTTACCGTTCCAGTGAAAGCGCAGTCTCTGTTTTT
<i>CO-B-R4-6T</i>	TTTTTTGGTTTAGTACCGCCACATCACCGTACTCAGGATTTTTT
<i>CO-B-R5-6T</i>	TTTTTTACTAAAGGAATTGCGAAGAATAGAAAGGAACA
<i>CO-B-R6-6T</i>	TTTTTTGAGGACTAAAGACTTTCGGCTACAGAGGCTTT
<i>CO-B-D1-RQ</i>	/5IAbRQ/TTACGGTTAATAAGAATAAAGTGTGATAAATAAGGC
<i>CO-B-D2</i>	ATGTCAAATCGTCGCTATTAATAACCTTGCTTCTGT
<i>CO-B-D3</i>	GATAGAAATAAAGAAATTGCGTTAGCACGTAAAACAGCAAGT
<i>CO-B-D4</i>	ACTCATATTCCTGATTATCAGAGCGGAATTATCATCAGTAGA
<i>CO-B-D5</i>	TGCTGAACCTCAAATAATCTAAAGCATCACCTTGAAC
<i>CO-B-D6-Cy5</i>	ACATTGGCAGATTCACCTGAAATGGATTATTT/iCy5/ACACT

Table A.4. 2-2 Dimer A-Tile Edge Staple Sequences

Name	Sequence
<i>CO-A-R1-RQ</i>	/5IAbRQ/CTGTTGTTAAATAAGAATAAAGTGTGATAAATAAGGC
<i>CO-A-R2</i>	CGAATAAATCGTCGCTATTAATAACCTTGCTTCTGT
<i>CO-A-R3</i>	GTCTTAAATAAAGAAATTGCGTTAGCACGTAAAACAGAAGGT
<i>CO-A-R4</i>	ATCCTTATTCCTGATTATCAGAGCGGAATTATCATCATATGG
<i>CO-A-R5</i>	TGCTGAACCTCAAATAATCTAAAGCATCACCTGCAAA
<i>CO-A-R6-Cy5</i>	ACATTGGCAGATTCACCTGAAATGGATTATTT/iCy5/AGCAT
<i>CO-A-D1-6T</i>	TTTTTCGTTAATATTTTGTTAATATTTAAATTGTAAA
<i>CO-A-D2-6T</i>	TTTTTTGAGTAATGTGTAGGTTTTTAAATGCAATGCC
<i>CO-A-D3-6T</i>	TTTTTTATTAGATACATTTTCGCTAGATTTAGTTTGACCTTTTTT
<i>CO-A-D4-6T</i>	TTTTTTATCAAAAAGATTAAGAAAGCAAAGCGGATTGCTTTTTT
<i>CO-A-D5-6T</i>	ATAACGCCAAAAGGAACAATAATGCAGATACTTTTTT
<i>CO-A-D6-6T</i>	GGATATTCATTACCCAATCTTCGACAAGAACCTTTTTT
<i>CO-A-L1-6T</i>	TCCTGAACAAGAAAAAATCAACAATAGATAAGTTTTT
<i>CO-A-L2-6T</i>	TTGCACCCAGCTACAAAAGATTAGTTGCTATTTTTTTT
<i>CO-A-L3-6T</i>	TTTTTTAATAATAAGAGCAAGAGAATTGAGTTAAGCCCTTTTTT
<i>CO-A-L4-6T</i>	TTTTTTGTTTGAGGGGACGACGAACCGTGCATCTGCCATTTTTT
<i>CO-A-L5-6T</i>	TTTTTTCCCGGGTACCGAGGTCTCGACTCTAGAGGATC
<i>CO-A-L6-6T</i>	TTTTTTAGCTGATTGCCCTTCACAGTGAGACGGGCAAC
<i>CO-A-U1-6T</i>	AATAAGTTTATTTTGTGCGCAAAGACACCACGGTTTTTTT
<i>CO-A-U2-6T</i>	TGTAGCGGTTTTTCATGCCTTTAGCGTCAGACTTTTTT
<i>CO-A-U3-6T</i>	TTTTTTAATTTACCGTTCCAGTGAAAGCGCAGTCTCTGTTTTTT
<i>CO-A-U4-6T</i>	TTTTTTGGTTTAGTACCGCCACATCACCGTACTCAGGATTTTTT
<i>CO-A-U5-6T</i>	TTTTTTACTAAAGGAATTGCGAAGAATAGAAAGGAACA
<i>CO-A-U6-6T</i>	TTTTTTGAGGACTAAAGACTTTCGGCTACAGAGGCTTT

Table A.5. 2-2 Dimer B-Tile Edge Staple Sequences

Name	Sequence
<i>CO-B-L1-Cy5</i>	AACAG/iCy5/CGTTAATATTTTGTTAATATTTAAATTGTAAA
<i>CO-B-L2</i>	ATTCGTGAGTAATGTGTAGGTTTTTAAATGCAATGCC
<i>CO-B-L3</i>	AAGACATTAGATACATTTTCGCTAGATTTAGTTTGACCACCTT
<i>CO-B-L4</i>	AGGATATCAAAAAGATTAAGAAAGCAAAGCGGATTGCCATA
<i>CO-B-L5</i>	ATAACGCCAAAAGGAACAACACTAATGCAGATACTTTGC
<i>CO-B-L6-RQ</i>	GGATATTCATTACCCAATCTTCGACAAGAACCATGCT/3IAbRQSp/
<i>CO-B-U1-6T</i>	TCCTGAACAAGAAAAATCAACAATAGATAAGTTTTT
<i>CO-B-U2-6T</i>	TTGCACCCAGCTACAAAAGATTAGTTGCTATTTTTTTT
<i>CO-B-U3-6T</i>	TTTTTTAATAATAAGAGCAAGAGAATTGAGTTAAGCCCTTTTTT
<i>CO-B-U4-6T</i>	TTTTTTGTTTGAGGGGACGACGAACCGTGCATCTGCCATTTTTT
<i>CO-B-U5-6T</i>	TTTTTTCCCGGTACCGAGGTCTCGACTCTAGAGGATC
<i>CO-B-U6-6T</i>	TTTTTTAGCTGATTGCCCTTCACAGTGAGACGGGCAAC
<i>CO-B-R1-6T</i>	AATAAGTTTATTTTGTGCAAAGACACCACGGTTTTTTT
<i>CO-B-R2-6T</i>	TGTAGCGCGTTTTTCATGCCTTTAGCGTCAGACTTTTTT
<i>CO-B-R3-6T</i>	TTTTTTAATTTACCGTTCCAGTGAAAGCGCAGTCTCTGTTTTT
<i>CO-B-R4-6T</i>	TTTTTTGGTTTAGTACCGCCACATCACCGTACTCAGGATTTTTT
<i>CO-B-R5-6T</i>	TTTTTTACTAAAGGAATTGCGAAGAATAGAAAGGAACA
<i>CO-B-R6-6T</i>	TTTTTTGAGGACTAAAGACTTTCGGCTACAGAGGCTTT
<i>CO-B-D1-6T</i>	TTTTTTGTTAAATAAGAATAAAGTGTGATAAATAAGGC
<i>CO-B-D2-6T</i>	TTTTTTAAATCGTCGCTATTAATAACCTTGCTTCTGT
<i>CO-B-D3-6T</i>	TTTTTTAAATAAAGAAATTGCGTTAGCACGTAAACAGTTTTTTT
<i>CO-B-D4-6T</i>	TTTTTTTATTCTGATTATCAGAGCGGAATTATCATCATTTTTT
<i>CO-B-D5-6T</i>	TGCTGAACCTCAAATAATCTAAAGCATCACCTTTTTTTT
<i>CO-B-D6-6T</i>	ACATTGGCAGATTCACCTGAAATGGATTATTTTTTTTTT

Table A.6. 2x2 Array A-Tile Edge Staple Sequences

Name	Sequence
<i>CO-A-R1-RQ</i>	/5IAbRQ/CTGTTGTTAAATAAGAATAAAGTGTGATAAATAAGGC
<i>CO-A-R2</i>	CGAATAAATCGTCGCTATTAATAACCTTGCTTCTGT
<i>CO-A-R3</i>	GTCTTAAATAAAGAAATTGCGTTAGCACGTAAAACAGAAGGT
<i>CO-A-R4</i>	ATCCTTATTCCTGATTATCAGAGCGGAATTATCATCATATGG
<i>CO-A-R5</i>	TGCTGAACCTCAAATAATCTAAAGCATCACCTGCAAA
<i>CO-A-R6-Cy5</i>	ACATTGGCAGATTCACCTGAAATGGATTATTT/iCy5/AGCAT
<i>CO-A-D1-Cy5</i>	CGTAA/iCy5/CGTTAATATTTTGTTAATATTTAAATTGTAAA
<i>CO-A-D2</i>	GACATTGAGTAATGTGTAGGTTTTTAAATGCAATGCC
<i>CO-A-D3</i>	CTATCATTAGATACATTTTCGCTAGATTTAGTTTGACCACTTG
<i>CO-A-D4</i>	TGAGTATCAAAAAGATTAAGAAAAGCAAAGCGGATTGCTCTAC
<i>CO-A-D5</i>	ATAACGCCAAAAGGAACAATAATGCAGATACGTTCA
<i>CO-A-D6-RQ</i>	GGATATTCATTACCCAATCTTCGACAAGAACCAGTGT/3IAbRQSp/
<i>CO-A-L1-6T</i>	TCCTGAACAAGAAAAAATCAACAATAGATAAGTTTTT
<i>CO-A-L2-6T</i>	TTGCACCCAGCTACAAAAGATTAGTTGCTATTTTTTTT
<i>CO-A-L3-6T</i>	TTTTTTAATAATAAGAGCAAGAGAATTGAGTTAAGCCCTTTTTT
<i>CO-A-L4-6T</i>	TTTTTTGTTTGAGGGGACGACGAACCGTGCATCTGCCATTTTTT
<i>CO-A-L5-6T</i>	TTTTTTCCCGGGTACCGAGGTCTCGACTCTAGAGGATC
<i>CO-A-L6-6T</i>	TTTTTTAGCTGATTGCCCTTCACAGTGAGACGGGCAAC
<i>CO-A-U1-6T</i>	AATAAGTTTATTTTGTGCGCAAAGACACCACGGTTTTTTT
<i>CO-A-U2-6T</i>	TGTAGCGGTTTTTCATGCCTTTAGCGTCAGACTTTTTT
<i>CO-A-U3-6T</i>	TTTTTTAATTTACCGTTCCAGTGAAAGCGCAGTCTCTGTTTTTT
<i>CO-A-U4-6T</i>	TTTTTTGGTTTAGTACCGCCACATCACCGTACTCAGGATTTTTT
<i>CO-A-U5-6T</i>	TTTTTTACTAAAGGAATTGCGAAGAATAGAAAGGAACA
<i>CO-A-U6-6T</i>	TTTTTTGAGGACTAAAGACTTTCGGCTACAGAGGCTTT

Table A.7. 2x2 Array B-Tile Edge Staple Sequences

Name	Sequence
<i>CO-B-L1-Cy5</i>	AACAG/iCy5/CGTTAATATTTTGTTAATATTTAAATTGTAAA
<i>CO-B-L2</i>	ATTCGTGAGTAATGTGTAGGTTTTTAAATGCAATGCC
<i>CO-B-L3</i>	AAGACATTAGATACATTTTCGCTAGATTTAGTTTGACCACCTT
<i>CO-B-L4</i>	AGGATATCAAAAAGATTAAGAAAGCAAAGCGGATTGCCATA
<i>CO-B-L5</i>	ATAACGCCAAAAGGAACAACACTAATGCAGATACTTTGC
<i>CO-B-L6-RQ</i>	GGATATTCATTACCCAATCTTCGACAAGAACCATGCT/3IAbRQSp/
<i>CO-B-U1-6T</i>	TCCTGAACAAGAAAAATCAACAATAGATAAGTTTTT
<i>CO-B-U2-6T</i>	TTGCACCCAGCTACAAAAGATTAGTTGCTATTTTTTTT
<i>CO-B-U3-6T</i>	TTTTTTAATAATAAGAGCAAGAGAATTGAGTTAAGCCCTTTTTT
<i>CO-B-U4-6T</i>	TTTTTTGTTTGAGGGGACGACGAACCGTGCATCTGCCATTTTTT
<i>CO-B-U5-6T</i>	TTTTTTCCCGGGTACCGAGGTCTCGACTCTAGAGGATC
<i>CO-B-U6-6T</i>	TTTTTTAGCTGATTGCCCTTTCACAGTGAGACGGGCAAC
<i>CO-B-R1-6T</i>	AATAAGTTTATTTTGTGCAAAGACACCACGGTTTTTTT
<i>CO-B-R2-6T</i>	TGTAGCGCGTTTTTCATGCCTTTAGCGTCAGACTTTTTT
<i>CO-B-R3-6T</i>	TTTTTTAATTTACCGTTCCAGTGAAAGCGCAGTCTCTGTTTTT
<i>CO-B-R4-6T</i>	TTTTTTGGTTTAGTACCGCCACATCACCGTACTCAGGATTTTTT
<i>CO-B-R5-6T</i>	TTTTTTACTAAAGGAATTGCGAAGAATAGAAAGGAACA
<i>CO-B-R6-6T</i>	TTTTTTGAGGACTAAAGACTTTCGGCTACAGAGGCTTT
<i>CO-B-D1-RQ</i>	/5IAbRQ/TTACGGTTAATAAGAATAAAGTGTGATAAATAAGGC
<i>CO-B-D2</i>	ATGTCAAATCGTCGCTATTAATAACCTTGCTTCTGT
<i>CO-B-D3</i>	GATAGAAATAAAGAAATTGCGTTAGCACGTAAAACAGCAAGT
<i>CO-B-D4</i>	ACTCATATCCTGATTATCAGAGCGGAATTATCATCAGTAGA
<i>CO-B-D5</i>	TGCTGAACCTCAAATAATCTAAAGCATCACCTTGAAC
<i>CO-B-D6-Cy5</i>	ACATTGGCAGATTCACCTGAAATGGATTATTT/iCy5/ACACT

Table A.8. UB Array A-Tile Edge Staple Sequences

Name	Sequence
<i>CO-A-R1-RQ</i>	/5IAbRQ/CTGTTGTTAAATAAGAATAAAGTGTGATAAATAAGGC
<i>CO-A-R2</i>	CGAATAAATCGTCGCTATTAATAACCTTGCTTCTGT
<i>CO-A-R3</i>	GTCTTAAATAAAGAAATTGCGTTAGCACGTAAAACAGAAGGT
<i>CO-A-R4</i>	ATCCTTATTCCTGATTATCAGAGCGGAATTATCATCATATGG
<i>CO-A-R5</i>	TGCTGAACCTCAAATAATCTAAAGCATCACCTGCAAA
<i>CO-A-R6-Cy5</i>	ACATTGGCAGATTCACCTGAAATGGATTATTT/iCy5/AGCAT
<i>CO-A-D1-Cy5</i>	CGTAA/iCy5/CGTTAATATTTTGTTAATATTTAAATTGTAAA
<i>CO-A-D2</i>	GACATTGAGTAATGTGTAGGTTTTTAAATGCAATGCC
<i>CO-A-D3</i>	CTATCATTAGATACATTTTCGCTAGATTTAGTTTGACCACTTG
<i>CO-A-D4</i>	TGAGTATCAAAAAGATTAAGAAAAGCAAAGCGGATTGCTCTAC
<i>CO-A-D5</i>	ATAACGCCAAAAGGAACAATAATGCAGATACGTTCA
<i>CO-A-D6-RQ</i>	GGATATTCATTACCCAATCTTCGACAAGAACCAGTGT/3IAbRQSp/
<i>CO-A-L1-Cy5</i>	TCCTGAACAAGAAAAAATCAACAATAGATAAG/iCy5/AGCAT
<i>CO-A-L2</i>	TTGCACCCAGCTACAAAAGATTAGTTGCTATTGCAAA
<i>CO-A-L3</i>	ATCCTAATAATAAGAGCAAGAGAATTGAGTTAAGCCCTATGG
<i>CO-A-L4</i>	GTCTTGTTTGAGGGGACGACGAACCGTGCATCTGCCAAAGGT
<i>CO-A-L5</i>	CGAATCCCGGGTACCGAGGTCTCGACTCTAGAGGATC
<i>CO-A-L6-RQ</i>	/5IAbRQ/CTGTTAGCTGATTGCCCTTCACAGTGAGACGGGCAAC
<i>CO-A-U1-RQ</i>	AATAAGTTTATTTTGTGCGCAAAGACACCACGGAGTGT/3IAbRQSp/
<i>CO-A-U2</i>	TGTAGCGGTTTTTCATGCCTTTAGCGTCAGACGTTCA
<i>CO-A-U3</i>	TGAGTAATTTACCGTTCCAGTGAAAGCGCAGTCTGTCTAC
<i>CO-A-U4</i>	CTATCGGTTTAGTACCGCCACATCACCGTACTCAGGAACTTG
<i>CO-A-U5</i>	GACATACTAAAGGAATTGCGAAGAATAGAAAGGAACA
<i>CO-A-U6-Cy5</i>	CGTAA/iCy5/GAGGACTAAAGACTTTTCGGCTACAGAGGCTTT

Table A.9. UB Array B-Tile Edge Staple Sequences

Name	Sequence
<i>CO-B-L1-Cy5</i>	AACAG/iCy5/CGTTAATATTTTGTTAATATTTAAATTGTAAA
<i>CO-B-L2</i>	ATTCGTGAGTAATGTGTAGGTTTTTAAATGCAATGCC
<i>CO-B-L3</i>	AAGACATTAGATACATTTTCGCTAGATTTAGTTTGACCACCTT
<i>CO-B-L4</i>	AGGATATCAAAAAGATTAAGAAAAGCAAAGCGGATTGCCATA
<i>CO-B-L5</i>	ATAACGCCAAAAGGAACAACACTAATGCAGATACTTTGC
<i>CO-B-L6-RQ</i>	GGATATTCATTACCCAATCTTCGACAAGAACCATGCT/3IAbRQSp/
<i>CO-B-U1-Cy5</i>	TCCTGAACAAGAAAAAATCAACAATAGATAAG/iCy5/ACACT
<i>CO-B-U2</i>	TTGCACCCAGCTACAAAAGATTAGTTGCTATTTGAAC
<i>CO-B-U3</i>	ACTCAAATAATAAGAGCAAGAGAATTGAGTTAAGCCCGTAGA
<i>CO-B-U4</i>	GATAGGTTTGAGGGGACGACGAACCGTGCATCTGCCACAAGT
<i>CO-B-U5</i>	ATGTCCCCGGGTACCGAGGTCTCGACTCTAGAGGATC
<i>CO-B-U6-RQ</i>	/5IAbRQ/TTACGAGCTGATTGCCCTTACAGTGAGACGGGCAAC
<i>CO-B-R1-RQ</i>	AATAAGTTTATTTTGTGCGAAAGACACCACGGATGCT/3IAbRQSp/
<i>CO-B-R2</i>	TGTAGCGCGTTTTTCATGCCTTTAGCGTCAGACTTTGC
<i>CO-B-R3</i>	AGGATAATTTACCGTTCCAGTGAAAGCGCAGTCTCTGCCATA
<i>CO-B-R4</i>	AAGACGGTTTAGTACCGCCACATCACCGTACTCAGGAACCTT
<i>CO-B-R5</i>	ATTCGACTAAAGGAATTGCGAAGAATAGAAAGGAACA
<i>CO-B-R6-Cy5</i>	AACAG/iCy5/GAGGACTAAAGACTTTTCGGCTACAGAGGCTTT
<i>CO-B-D1-RQ</i>	/5IAbRQ/TTACGGTTAAATAAGAATAAAGTGTGATAAATAAGGC
<i>CO-B-D2</i>	ATGTCAAATCGTCGCTATTAATAACCTTGCTTCTGT
<i>CO-B-D3</i>	GATAGAAATAAAGAAATTGCGTTAGCACGTAAAACAGCAAGT
<i>CO-B-D4</i>	ACTCATATTCCTGATTATCAGAGCGGAATTATCATCAGTAGA
<i>CO-B-D5</i>	TGCTGAACCTCAAATAATCTAAAGCATCACCTTGAAC
<i>CO-B-D6-Cy5</i>	ACATTGGCAGATTCACCTGAAATGGATTATTT/iCy5/ACACT

APPENDIX D

DNA Origami Annealing Protocol**Table A.10. Origami Cross Tile Annealing Protocol**

Step #	Temperature and Rate
1	Increase to 70° C at a rate of 1° C / 18 sec
2	Hold 70° C for 50 minutes
3	Decrease to 60° C at 1° C / 450 sec
4	Decrease to 55° C at 1° C / 600 sec
5	Decrease to 50° C at 1° C / 900 sec
6	Decrease to 35° C at 1° C / 1200 sec
7	Decrease to 30° C at 1° C / 240 sec
8	Decrease to 20° C and hold
9	End Anneal